UNIVERSIDADE DE LISBOA
FACULDADE DE CIÊNCIAS
DEPARTAMENTO DE ENGENHARIA GEOGRÁFICA, GEOFÍSICA E ENERGIA

Identification of the magnetic external component in annual and monthly means of magnetic observatory data series

Diana Filipa Lourenço Saturnino

Mestrado em Ciências Geofísicas

Especialização em Geofísica Interna

2012

UNIVERSIDADE DE LISBOA
FACULDADE DE CIÊNCIAS
DEPARTAMENTO DE ENGENHARIA GEOGRÁFICA, GEOFÍSICA E ENERGIA

Identification of the magnetic external component in annual and monthly means of magnetic observatory data series

Diana Filipa Lourenço Saturnino

Mestrado em Ciências Geofísicas

Especialização em Geofísica Interna

Trabalho de Projecto orientado pelos

Prof. Doutor Miguel Miranda (FCUL) e Prof. Doutora Alexandra Pais (FCTUC)

2012

It is the nature of geomagnetic fields to not divulge their sources simply.

(Campbell, 2003)

I would like to express my gratitude to my advisor, Dr. Prof Alexandra Pais. This work was only possible because of her orientation and guidance. During all this time, she was always present to clarify my doubts, give advices and ideas; she helped me writing this dissertation and ultimately, taught me how to make science. Thanks.

I would also like to thank Anna Morozova, for her insights and advices on the treatment of data series.

The results presented in this paper rely on data collected at magnetic observatories. I thank the national institutes that support them and INTERMAGNET for promoting high standards of magnetic observatory practice (*www.intermagnet.org*).

This work allowed testing the application of the EOF analysis to geomagnetic data. Its conclusions will be important to the project PTDC/CTE-GIX/119967/2010.

Resumo

O campo geomagnético medido nos observatórios magnéticos à superfície da Terra contém contribuições de fontes internas (núcleo líquido e litosfera) e também de fontes acima da superfície terrestre que originam a componente externa. Esta componente externa deve-se a vários sistemas de correntes eléctricas presentes na ionosfera e na magnetosfera. A origem dessas corentes está directa ou indirectamente ligada à actividade solar e à interacção dinâmica entre o Sol e o ambiente em torno da Terra. A iluminação solar diária cria uma maré térmica que, por sua vez, origina correntes de plasma no hemisfério iluminado da ionosfera, designadas por "variabilidade solar (solar-quiet day, *Sq*)" e o jacto equatorial (EEJ), dominante nas médias e pequenas latitudes. Para além destas correntes existem outras nas regiões polares, os jactos polares (PEJ ou AEJ), que consistem em correntes eléctricas horizontais que circulam na camada E da ionosfera, acima da região polar. A interacção entre o vento solar e o campo magnético da Terra gera a corrente da magnetopausa e o anel de corrente. A primeira é responsável pelo cancelamento do campo magnético terrestre fora da magnetosfera e circula principalmente do nascer do Sol para o pôr do Sol no lado diurno e nosentido contrário no lado nocturno, onde se designa por corrente de cauda ("tail current"). O anel de corrente consiste num deslocamento de electrões e iões na cintura do equador geomagnético, de este para oeste, a uma distância da Terra de 3 a 6 raios terrestres (R_E), e é fortemente dependente da actividade solar. Correntes adicionais estão presentes na ionosfera e magnetosfera, tais como as correntes alinhadas ("field-aligned currents"), que circulam a partir do equador na magnetosfera para as latitudes altas na ionosfera. Estas correntes têm duas regiões de maior acção: Região 1, em redor da zona polar e Região 2, principalmente na zona equatorial. O intuito deste trabalho é identificar nos dados dos observatórios magnéticos a variabilidade temporal e espacial associadas a estas correntes externas que afectam o campo magnético medido à superfície da Terra. Para tal, a contribuição externa do campo foi isolada em médias mensais e anuais de dados de observatórios magnéticos (da rede INTERMAGNET), para cinco componentes magnéticas (X, Y, Z, H e F) e para dois períodos de tempo: 1963-2001 e 1985-1989. No primeiro intervalo de tempo utilizaram-se dados de 23 observatórios, espalhados pelo globo; já no segundo intervalo de tempo utilizaram-se dados de 56 observatórios. Estas escolhas foram determinadas pela ideia de testar a dependência dos resultados relativamente à escolha dos intervalos temporal e espacial. Após o pré-processamento dos dados, o isolamento da componente externa foi obtido por subtracção da contribuição do campo principal (núcleo líquido), dada pelo modelo CM4 (Comprehensive Model 4), às médias mensais e anuais, para cada observatório. Os resultados obtidos, que consistem na componente externa do campo, designaram-se por resíduos. De seguida, o método de análise de Funções Empíricas Ortogonais (EOF) foi utilizado para cada conjunto de resíduos (ou seja, para cada uma das componentes magnéticas). Este método de análise permite identificar os padrões espaciais globais (funções empíricas ortogonais) e as funções de variação temporal (componentes principais) dos principais modos de variabilidade responsáveis por cada uma da componentes do campo magnético externo. Cada modo de variação temporal e espacial pode depois ser comparado e possivelmente relacionado com uma corrente específica ou um conjunto de correntes acopladas. O método permite, ao fim e ao cabo, reduzir a dimensionalidade do sistema para apenas alguns modos, que poderão ser relacionados com determinados processos dinâmicos e/ou físicos. Na sua essência, é um método exploratório (não necessita de qualquer modelização prévia), que decompõe os dados (com variáveis correlacionadas entre si) numa base de funções ortogonais (não correlacionadas) determinadas pelos dados em si. Apenas as componentes X, Y e Z originaram resultados significativos, devido ao facto de as restantes componentes, H e F, dependerem directamente das outras três componentes. As componentes principais (PCs) que foram obtidas foram comparadas com várias séries temporais de indices magnéticos (Dst, aa, AE, PC, ASY e SYM) e também com a série temporal do número de manchas solares (SSN). Por seu lado, as funções empíricas ortogonais (EOFs) foram comparados com um modelo analítico do anel de corrente e também com os resultados dados pelo CM4 para os campos devidos às correntes magnetosféricas e ionosféricas. Estas comparações tiveram como objectivo a identificação das correntes externas ou processos associados a correntes externas mais importantes

para a variabilidade temporal e espacial dos resíduos de cada componente magnética à superfície da Terra. As comparações com as séries temporais de indices magnéticos permitiram identificar as correntes/processos importantes para a variabilidade temporal. As comparações entre os padrões espaciais dos EOFs e os padrões espaciais do modelo de anel de corrente e campos magnetosférico e ionosférico do CM4, permitiram a identificação das correntes/processos importantes para a variabilidade espacial. Os resultados mais interessantes são: a maior parte dos resíduos das componentes magnéticas têm a sua variabilidade explicada pelos dois primeiros modos de variabilidade, alguns deles (essencialmente os referentes a médias anuais do menor intervalo de tempo) são praticamente explicados apenas pelo primeiro. Ou seja, o modo 1 explica 40%, 60% e até mais que 90% da variabilidade, enquanto o modo 2 explica desde apenas 0.24% até quase 30%. O anel de corrente é um processo importante na variabilidade da componente externa, pois influencia fortemente a variação espacial da componente Y. Além disso, a variação temporal da componente X está fortemente correlacionada com a variação temporal do anel de corrente. No entanto, os EOFs da componente X apresentam uma assimetria latitudinal em relação ao equador geomagnético, contrária ao que se esperava se o anel de corrente fosse a principal contribuição para esta componente. Ainda, as PCs da componente X correlacionam-se muito bem com os indices magnéticos associados às correntes polares e correntes alinhadas, o que sugere que a variabilidade desta componente também depende fortemente das correntes polares e das correntes alinhadas nas altas latitudes (principalmente no hemisférico Norte). Os EOFs da componente Z apresentam um padrão não relacionado com o anel de corrente nem com os campos magnetosférico e ionosférico. Esse padrão consiste em amplitudes de sinais opostos no hemisfério oeste e este, relativamente ao meridiano de Greenwich, o que leva a pensar que a variabilidade desta componente poderá estar ligada a correntes induzidas no oceano Atlântico. As elevadas correlações entre vários índices magnéticos e as PCs levantam a questão sobre se uma parametrização da variação temporal da componente externa nos modelos actuais apenas à custa do índice Dst não será muito simplista e enganadora. Outros resultados foram obtidos, como a identificação em vários EOFs de um padrão de grande amplitude na região da América do Sul que poderá estar relacionado com a Anomalia do Atlântico Sul (SAA), levantando a questão sobre se a subtracção do sinal interno foi eficaz na remoção desta anomalia ou, então, se a variação temporal desta anomalia induz correntes que contribuem para a componente externa do campo. A existência do sinal do jerk de 1969 em PCs da componente Y, levanta igualmente a questão acerca da correcta subtracção da componente interna do campo.

Palavras-chave: Campo Magnético Terrestre, Observatórios magnéticos, Componente Externa, Índices Geomagnéticos, Funções Empíricas Ortogonais (EOF).

Abstract

The magnetic field measured by ground-based observatories has a contribution not only from internal (liquid core and crustal) sources but also from sources above the Earth's surface which give rise to the external component. This external component is due to a number of electrical currents in the magnetosphere-ionosphere system, whose sources are directly or indirectly related to the dynamical interaction between the Sun and the Earth's environment. The Sun daily illumination creates a thermic tide which generates plasma currents in the day side ionosphere, known as "solar-quiet day" (S_q) and equatorial electrojet, dominant in mid- and low latitudes. Furthermore, there are current systems in the polar regions, the auroral or polar electrojets, which are horizontal electric currents flowing in the E-region auroral belts. The interaction between the solar wind and the Earth's magnetic field generates the magnetopause current and the ring current. The first one flows primarily from dawn to dusk sunwards, and from dusk to dawn in the nightside, where it is called the tail current. The ring current consists on a drift of electrons and ions in the radiation belt flowing westward around the Earth at a distance between 3 and 6 Earth radius (R_E), strongly dependent on the solar activity. Additional magnetosphere-ionosphere currents are present, like the field-aligned currents (from the equatorial magnetosphere to high-latitude ionosphere) with two main regions of action: Region 1, more poleward and Region 2, more equatorward. In this study, and in order to identify the variability associated to different external current affecting the magnetic field at the Earth's surface, the external component was isolated from the magnetic observatory annual and monthly means of five magnetic components (X, Y, Z, H and F) during two time intervals: 1963-2001 and 1968-1990. That was done by subtracting the main field (liquid core) contribution given by the CM4 model on each observatory. Then the Empirical Orthogonal Function analysis was used on the components of the residuals. This method allows one to identify the spatial global pattern (empirical orthogonal functions) and the temporal function variation (principal components) of the major variability modes responsible for each component of the external field. Each mode of spatial and temporal variation can hopefully be related with a specific current or a set of coupled currents. Only the X, Y and Z components provided significant results, as the H and F components depend on the other three. The principal components were compared with geomagnetic indices time series (Dst, aa, AE, PC, ASY and SYM) and with the sunspot number data series. The empirical functions where compared with an analytical model for the ring current and with the results of the magnetospheric and ionospheric field components from the CM4 model. These comparisons allowed one to identify the external currents and/or processes associated to external currents which are more important to the time and spatial variability of each component of magnetic residuals, measured at the Earth's surface. Main interesting results are: the ring current is not the only important source explaining the variability of the external component currents in auroral and polar latitudes, and also the field-aligned currents are seemingly more important; the Z component spatial variability could be related with induced currents in the Atlantic Ocean; and also, using only but the Dst time series to parameterize the temporal variation of the external sources shows to be a too simplistic approach.

Key words: geomagnetic field, magnetic observatories, external component, geomagnetic indices, Empirical Orthogonal Functions (EOF).

Index

List of figures

List of Tables

1. Introduction

One of the most important goals of the study of the Earth's Magnetic Field is the qualitative and quantitative description of its various sources. Understanding the exact behaviour of each source and its importance in the whole magnetic system would allow one to fully explain the entire geomagnetic field and to predict its future behaviour. But that is a difficult and ongoing task, mostly due to the inaccessibility to the main source of the magnetic field itself, the Earth's liquid core, and also because the observations at the Earth's surface are a mixture of contributions from several sources, with spatial and temporal scales difficult to separate.

There are various approaches to the problem, usually in the form of magnetic field models. Geomagnetic observatories on the ground have been measuring the field for almost two hundred years, on a regular basis. But their spatial distribution is rather uneven, with large gaps in the oceans and the European region over-represented compared to the rest of Earth. However, during the last two decades the satellite missions made available a true global survey of geomagnetic field measurements, which helped the computation of magnetic field models. Different models use slightly different methods. The main field is modelled as a gradient of a scalar potential of internal origin, which in spherical coordinates makes use of spherical harmonics and Gauss coefficients. The external contributions are parameterized, like in the IGRF (International Geomagnetic Reference Field) and the CM (Comprehensive Models) models. They differ in the data type and the maximum degree of the involved Gauss coefficients used and in the choice of the temporal and spatial processes to be modelled. The IGRF models, like the latest IGRF11 (IAGA, Working Group V-MOD, 2010) give the main field and its secular variation at any point of the Earth's surface for a given time span. Comprehensive models, like CM4 (Sabaka et al, 2002; Sabaka et al, 2004), use parameterization and co-estimation of fields associated with major external current sources from field measurements taken from ground-based observatories and by satellite missions (Sabaka et al, 2004). These models compute separate fields corresponding to those of the core, lithospheric, ionospheric and magnetospheric origin along with associated induced currents and toroidal fields. Other models try to parameterize not the main field but the external contribution sources, using satellite data, like the ones from Tsyganenko (Tsyganenko, 1996, Tsyganenko and Stinov, 2007).

Nevertheless, all these models use parameterizations for the external sources. These require assumptions about the geometry and temporal variability of the source currents. As a negative side effect, they constrain the model with sometimes arguable assumptions and remove much of the above mentioned variability. One way to know and study the (hopefully) real temporal and spatial variability of the external currents is using the statistical method of Empirical Orthogonal Functions (EOF). This method, in its essence, is a way to reduce the dimensionality of the original data, without compromising much of the explained variance (Hannachi et al, 2007). The analysis is then used to

extract individual modes of variability of the data; however these modes are statistical and a physical interpretation has to be made with extreme caution. EOF analysis was first used in meteorology and oceanography and has been very popular in these fields (Obukhov, 1947; Lorenz, 1956; Barbosa and Andersen, 2009; for a review see Hannachi et al, 2007; and for a textbook see Preisendorfer, 1988). An important feature of the method is that it does not need *a priori* parameters or assumptions, the results come from the data itself.

Recently, this technique has also been also used for geomagnetic studies: Balasis and Egbert (2006) apply it to mid-latitude night-side hourly mean geomagnetic observatory data to search for evidence of non-zonal low-frequency (asymmetric magnetospheric) source fields. Lyakhov and Khlybov (2006) use the EOF analysis to the total electron content (TEC) in the Earth's ionosphere and perform an unbiased separation of the components of variability of that medium caused by solar and magnetic activity. Natali and Meza (2011) apply it to global vertical TEC (VTEC) during high solar activity and analyse the annual, semiannual and seasonal temporal and spatial variability of the ionosphere.

The aim of this work is to find the most important spatial and temporal modes of variability of the electric currents in the ionosphere and magnetosphere, the sources for the external component of the geomagnetic field, through EOF analysis of annual and monthly means of magnetic observatory data subtracted from a model for the main field. It also aims to discuss the importance of the temporal and spatial size of the data set used in the analysis. For that, two data sets where chosen, one with a better spatial distribution of the ground based observatories and with a few years of data, and the other data set with a poorer spatial distribution but a longer temporal series. After applying the EOF analysis both on annual and monthly means residuals (obtained when subtracting the mean value and the main field contribution given by the CM4 model on each observatory) to the two data sets, the resulting temporal and spatial modes of variability obtained were compared with an analytical model for the external ring current and with the results of different field components from the CM4 model.

This report is organized as follows. Section 2 presents an introduction to the subject of the Earth's magnetic field, with focus on the external component of the field and their sources. Geomagnetic indices are also introduced. The EOF analysis is the theme of section 3. Application of the method is presented in the section 4 and the results are shown in section 5. Section 6 presents the discussion on the results and the comparison with geomagnetic indices and magnetic models. Finally, in section 7 the general conclusions are drawn.

2. The Earth's Magnetic Field

The Earth's magnetic field, also known as geomagnetic field, is a very complex phenomenon, with several magnetic contributions due to different sources. Its strength varies at Earth's surface between approximately 25 000 nT around the magnetic equator and around 65 000 nT near the magnetic poles (1 nT = 1 nanotesla = 10^{-9} T).

The dominant part of the field (≈ 95%) is due to dynamo action (electrical currents) in the outer fluid core and is known as *main* (or *core*) field. The maximum intensity of the main field is around 60 000 nT near magnetic poles and around 25 000 nT near magnetic equator (Verbanac et al, 2010). Internal in origin is also the *lithospheric* or *crustal* field generated by magnetized material in the crust, accounting, on average, for only a few percentage of the total field but reaching locally hundreds or even thousands of nT close to Earth's surface. At satellite altitude the crustal field is much weaker, like < 30 nT at 400 km of altitude (Olsen and Stolle, 2012).

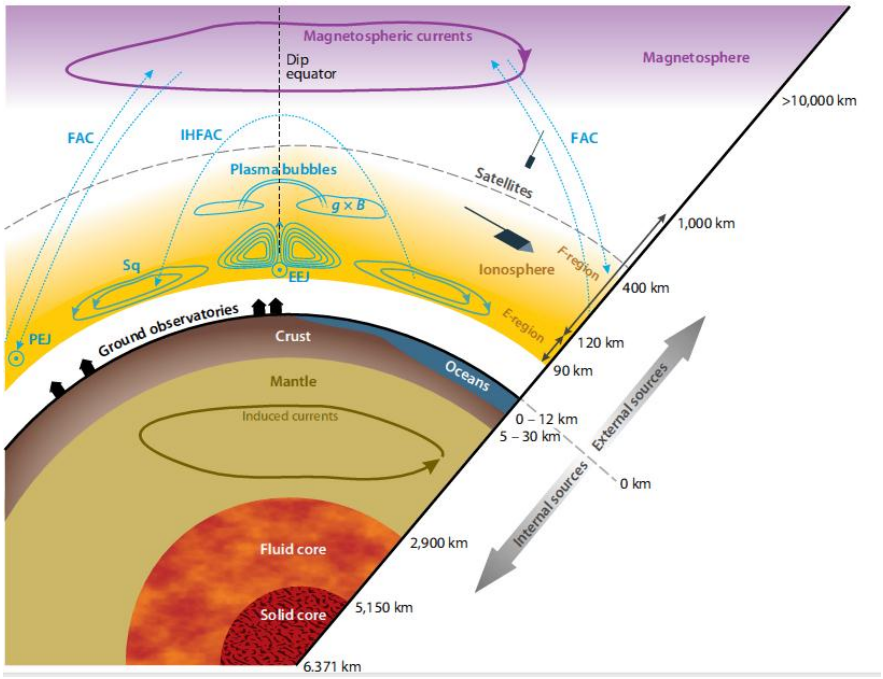

Figure 2.1. Sketch of the various sources contributing to the near-Earth magnetic field. An explanation of the abbreviations is given in the text. (From Olsen et al, 2012)

In addition to the internal sources there are contributions from several electric currents systems in the ionosphere (90 to 1 000 km altitude) and the magnetosphere (at distances larger than several Earth radii). These contributions are known as the *external* field (figure 2.1). The external sources are very dynamic, ranging from less than one nT during geomagnetically quiet conditions to several hundreds or even thousands of nT during disturbed times, with especially large amplitudes at polar latitudes (Olsen and Stolle, 2012). These external currents change continuously in time inducing secondary

currents in the Earth's interior (in the crust, more specifically), which, in turn, will produce a secondary induced magnetic contribution that adds to the primary external one.

It's essential to understand the processes behind internal and external sources of the geomagnetic field in order to separate their signatures (either by data selection or correction) when modelling each one separately. When studying the internal field, the external and/or the induced contributions are unwanted, but these same external contributions may be the interesting ones for those who study the ionosphere and magnetosphere.

The magnetic field measured at the ground observatories is a superposition of all internal and external contributions, each one with a spatial and temporal characteristic signature. The proper separation of the various contributions, based on magnetic measurements, is a major challenge. The usual way to achieve it is by means of spherical harmonic expansion, but is also used the filtering of data and data selection (Olsen and Stolle, 2012).

When the first time derivative of the data - called secular variation, SV - is calculated, some abrupt changes in the normally smooth trend are seen. These changes are called geomagnetic jerks and are more obvious in the Y component (see section 2.1), theoretically less contaminated by magnetospheric fields. Jerks have a typical "V" shape (figure 2.2) when the SV is approximated by a set of straight line segments dividing intervals of linear secular variation (Pinheiro and Jackson, 2008). The detection and characterization of jerks are still a topic of debate, more precisely their internal or external origin, their occurrence dates, their duration and their global or regional character (Mandea et al, 2010). The most well-known and studied jerk occurred in 1969 with a global behaviour. Many other jerks occurred, global or locally. Recent homogeneous satellite data as well as new magnetohydrodynamic models of the behaviour of the liquid core are helping the study on this subject.

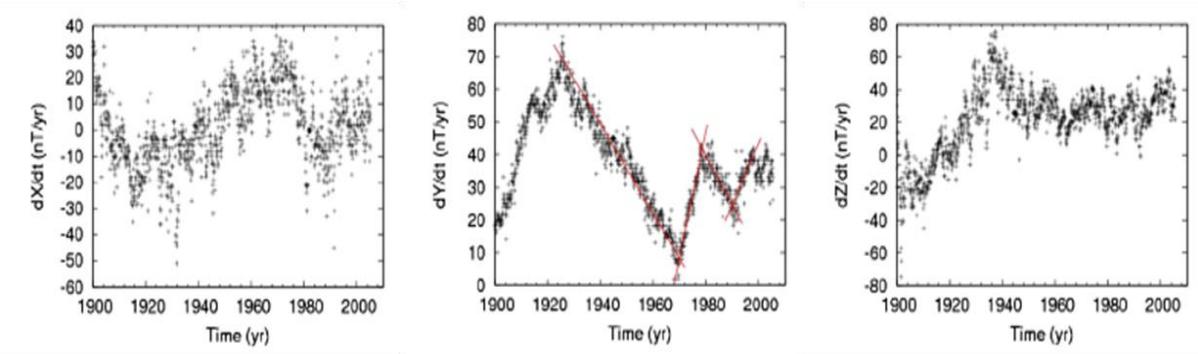

Figure 2.2. Secular variation for X, Y and Z components in the Niemegk (NGK) observatory. Times for three geomagnetic jerks, around 1969, 1978 and 1991 are indicated as intersections of successive straight-line segments with very different slopes, for the Y component (From Mandea et al. (2010)).

2.1 Magnetic components

The Earth's magnetic field measured on the surface is described by its components on a "right-hand system" and in a topocentric reference coordinate system (i.e. relative to a reference ellipsoid). These are called geodetic or topographic components. Figure 2.3 illustrates the nomenclature in use, with the total field vector pointing into the Earth as for a location on the Northern Hemisphere. Observers prefer to describe a vector representing the Earth's field in one of two ways (Campbell, 2003):

1) Three orthogonal component field directions with positive values for the geographic northward (X), eastward (Y) and vertical (Z) into the Earth (negative values for opposite directions, of course), or
2) The horizontal magnitude (H), the eastward (minus sign for westward) angular direction of the horizontal component from the geographic north (D, *declination*) and the downward (vertical) component (Z).

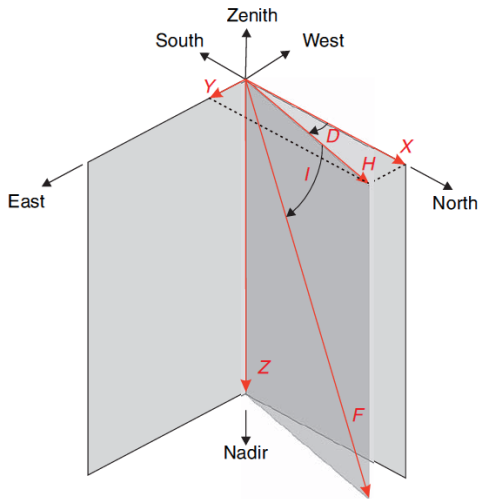

Figure 2.3.The magnetic components of the geomagnetic field on the Northern Hemisphere, seen from northeast.

The declination, the angle between the true north and the direction to which the compass needle points, was the important measure in the early days of navigation, so the HDZ system was the most used system in geomagnetic field measures. By simple geometry we can obtain the X and Y components from the H and D components:

$$X = H\cos(D),\ \ Y = \mathrm{H}\sin(D). \tag{2.1}$$

The total field strength, F, is given by

$$F = \sqrt{X^2 + Y^2 + Z^2} = \sqrt{H^2 + Z^2} \tag{2.2}$$

The angle I, called *inclination* (or dip angle) seen in figure 2.3, is the angle that the total field makes with the horizontal plane, and is given by

$$\frac{Z}{H} = \tan(I). \tag{2.3}$$

Again by simple geometry is easy to derive the H, D and I components of the field from the X, Y and Z components,

$$H = \sqrt{X^2 + Y^2}\,;\;\; D = \tan^{-1}\left(\frac{Y}{X}\right) \; and \; I = \; \tan^{-1}\left(\frac{Z}{H}\right). \tag{2.4}$$

In contrast to magnetic observations taken at or near ground and referred to geodetic coordinates, satellite data are typically provided in the spherical coordinates system where the three important directions are the angle (θ) measured from the North Pole along a great circle of longitude, the angle (ϕ) eastward along a latitude line measured from a reference latitude, and the radial direction (r) measured from the centre of the Earth. In the Earth's surface the field **B**, in spherical coordinates, is given by

$$B_\theta = -X'\,; \quad B_\phi = Y' \quad and \quad B_r = -Z'. \tag{2.5}$$

where, X', Y' and Z' are the geocentric coordinates. These are related with the geodetic coordinates (XYZ) through the following linear relations, with α been the angle between the radial direction measured from the Earth's centre (the B_r direction) and the vertical direction related to the geoid (the Z direction).

$$\begin{gathered} X = -B_\theta \cos(\alpha) - B_r \sin(\alpha) = X' \cos(\alpha) + Z' \sin(\alpha)\,; \\ Y = B_\phi = Y' \\ Z = \; B_\theta \sin(\alpha) - B_r \cos(\alpha) = -X' \sin(\alpha) + Z' \cos(\alpha). \end{gathered} \tag{2.6}$$

Originally, the HDZ system was used in most world observatories because the measuring instruments were suspended magnets and there was a direct application to navigation and land survey. However, the XYZ system is becoming the preferred coordinate system for most modern digital observatories.

2.2 The External Component of the field

The external component of the geomagnetic field is due to ionospheric and magnetospheric currents (which produce the primary field of external origin), and to the Earth-induced currents (which produce secondary externally induced internal fields). The contribution of these currents to the observed magnetic field, both at the ground and at satellite altitude is non-negligible. It is then of most importance to properly identify and separate their signal when studying the field of internal origin or the external field itself.

2.2.1 Ionospheric contributions

On some days, the magnetic records only display specific spectral period components (24, 12, 8 and 6 hours) which dominate the field registration. These records show oscillations similar to others seen in the past and following a seasonal cycle, known as *quiet daily geomagnetic variations*. Removing the lunar-tidal current system the remaining signal is called "*Sq*" for *solar quiet fields* (figure 2.4). These geomagnetic daily variations occur at nonpolar latitudes and are caused by diurnal wind systems in the ionosphere. Heating at the dayside and cooling at the night side generates thermospheric tidal winds which drive ionospheric plasma through the field lines of the ambient magnetic field (core field). This induces electric currents which, in turn, produce a magnetic field. Depending on the altitude and conditions of the process, it is common to distinguish between an E-region dynamo and an F-region dynamo.

The E-region (between 90 and 150 km altitude) current system, concentrated at an altitude of about 110-115 km, consists of two vortices (figure 2.4; see also figure 2.1) centred around local noon at ± 30 latitude, with anticlockwise (clockwise) currents in the Northern (Southern) Hemisphere. Typical peak-to-peak *Sq* amplitudes at middle latitudes are 20-50 nT. Amplitudes during solar maxima, i.e., during the hemispheric summer, are about twice as large as those during solar minimum. There is also a seasonal shift of the maximum (earlier in the summer and later in winter) for the *Sq* at middle and low latitude. The data from equatorial stations display a semiannual, equinoctial enhancement of amplitudes. Equatorial amplitudes of the daily variation *Sq*(D) and *Sq*(Z) are smaller than the one from H component. The daily pattern for the H component of the field seems to go through a transition in shape at middle latitudes, whereas the D components are reversed in direction for the Northern and Southern Hemispheres. When the seasons are matched, there seem to be some Northern/Southern Hemispheres differences in the quiet variations; for equivalent geomagnetic latitudes the fields seem more intense in the north (Campbell, 2003). Figure 2.5 illustrates conclusions about the source current shape that can be ascertained from surface field component records.

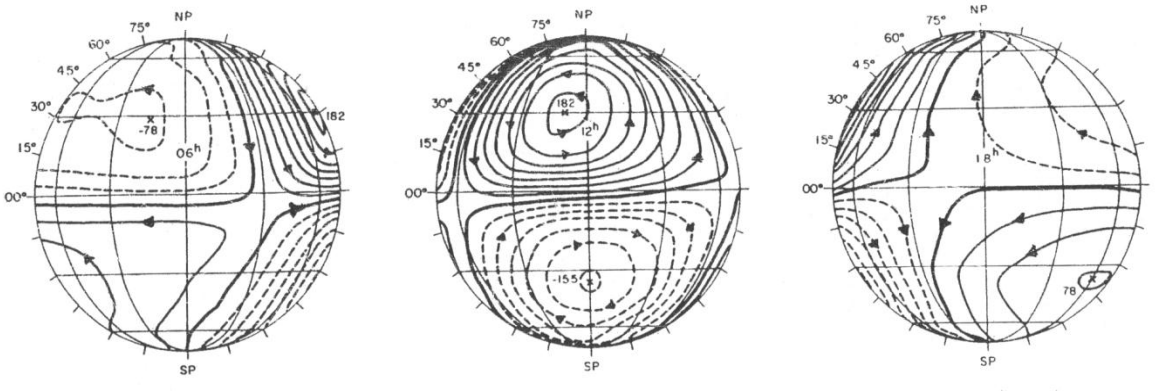

Figure 2.4. Yearly average Sq equivalent current system for 1958 viewed toward 06-, 12-, and 18-h meridians. Arrows indicate current flow direction. Clockwise contour are dashed, counterclockwise are solid. After Campbell (2003); figure from Matsushita (1967).

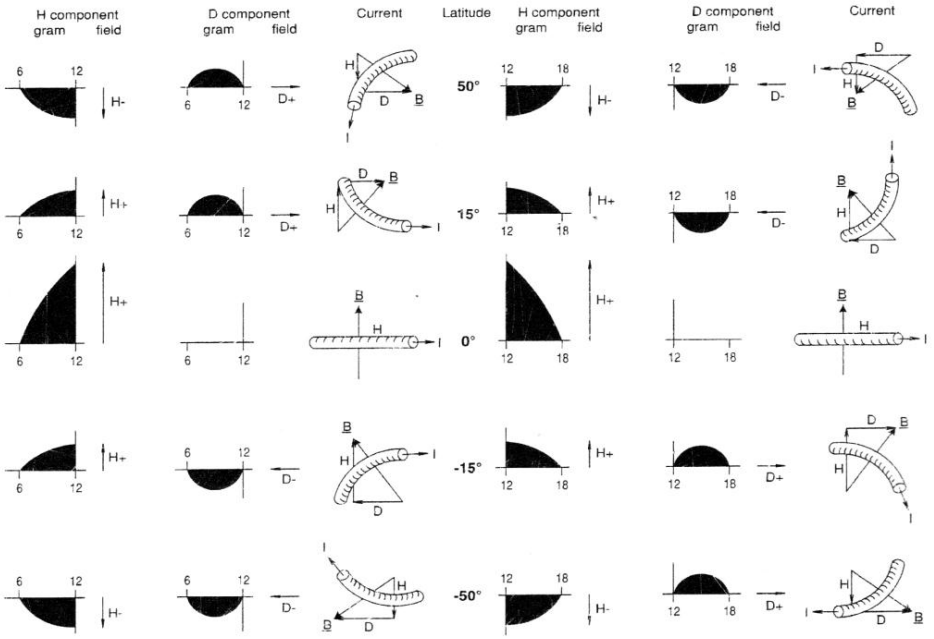

Figure 2.5. *Sq* current vortex patterns inferred from H and D field directions below 50° geomagnetic latitude. Morning patterns (06:00-12:00 local time) are shown on magnetograms to the left of the central latitude column; afternoon patterns (12:00-18:00 local time) are shown to the right. Variations for hours before and after 12:00 are indicated with arrows. Current in above-surface wire segments equivalent to cause the observed H and D fields are sketched to right of each H and D picture along with the B field vectors. The fields in the two hemispheres, at daytime, should be consistent with the *Sq* ionospheric current vortices depicted in figure 2.4. (From Campbell, 2003).

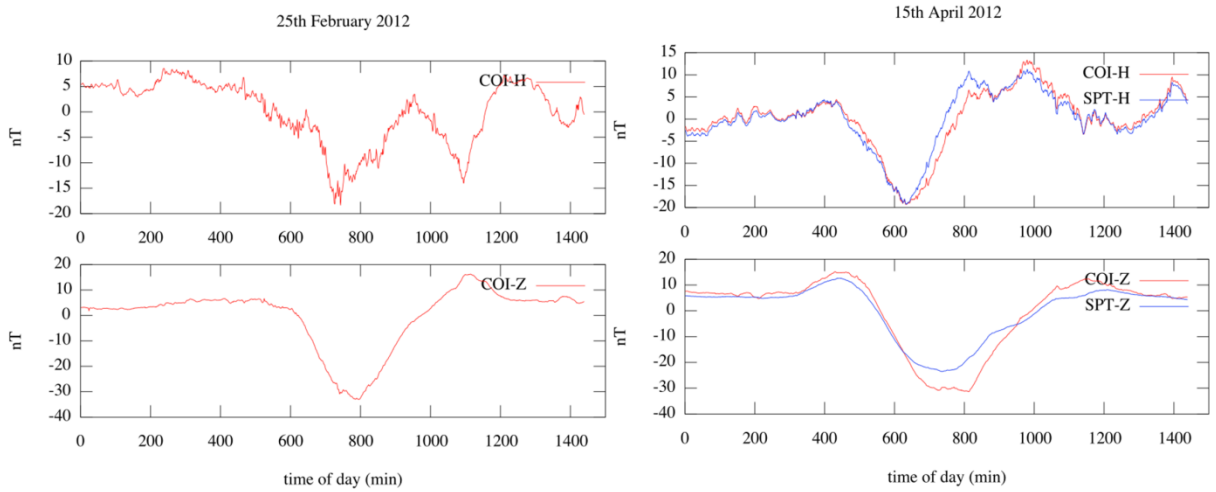

Figure 2.6. H and Z magnetic components for a winter (*left*) and spring (*right*) days on the COI (Coimbra, Portugal) and SPT (Toledo, Spain) observatories. The daily mean was subtracted, so the figure represents variations from the daily mean values. Only the spring days has the data for the two observatories. Notice that the scale of amplitudes in the H component is different in both days, the spring day shows an increase in amplitude. Also, the diurnal variation amplitude of the Z component is bigger in the COI observatory, despite the proximity of the latitudes (40.2° N in COI and 39.5°N in SPT). That could happen due to electrical currents in the Atlantic Ocean, closer to the COI observatory than the SPT.

Figure 2.6 shows the daily variation of the H and Z components for the Coimbra (Portugal) and Toledo (Spain) observatories for two days, one in the winter (February) and the other in the end of spring (April). The daily mean was subtracted and the time interval is one minute. The increase of the variation amplitude occurs in the spring day, as expected. The H component is more irregular than the Z component due to the summation of the external contributions. The H component daily variations seem to follow the ones from figure 2.5, with a strong decrease of amplitude (become more negative) after 06:00 local time and an increase after 12:00 local time.

Sq variations are restricted to the dayside hemisphere, and thus depend mainly on local time (figures 2.4 to 2.6). For example, in figure 2.6 is visible the change of amplitude during day hours and also the shift of the hour of maximum amplitude for the H component. When deriving models of the internal field is usual to select only the nightside data to minimize field contributions from the ionospheric E-region (Olsen et al, 2010).

On *magnetically disturbed* days there is an additional variation on the measured magnetic field. This variation includes superimposed magnetic storm signatures of magnetospheric and high-latitude ionospheric origin. For example, during magnetic storms, the H component decreases drastically.

As the geomagnetic field is strictly horizontal at the dip equator, there is an enhancement of the conductivity in the ionosphere dynamo region, which results in an enhanced eastward current, called *Equatorial Electrojet* (EEJ), flowing along the dayside dip equator. This EEJ is about 450 to 550 km wide, corresponding to a latitudinal width of about 6º to 8º.

Furthermore, there are complicated current systems in the polar regions. They are particularly strong during times of enhanced energy transfer from the sun into the magnetosphere but are always present (Olsen and Stolle, 2012). The auroral electrojets or *polar electrojets* (AEJ or PEJ) are horizontal electric currents flowing in the E-region auroral belts (near ± 65º-70º magnetic latitude). They vary widely in amplitude, giving different levels of magnetic activity from a few 100 nT during quiet periods to several thousand nT during major magnetic storms. Along with the AEJ, the polar ionosphere is also dominated by the *Field Aligned Currents* (FAC), electric currents flowing along the field lines of the ambient magnetic field and that connect the ionosphere with the magnetosphere. There are also, FAC that flow from one hemisphere to another, designated by interhemispheric field aligned currents (IHFAC). They were first proposed by van Sabben (1966) and unambiguously detected by Olsen (1997a) using satellite data.

Many other currents and/or irregularities exist in the ionosphere, like the equatorial plasma bubbles (see Kelley, 2009), the meridional current system in the low-latitude F-region (Heelis, 2004) and others (Olsen and Stolle, 2012). Contributions of currents in the ionospheric F-region, which extends from about 200 km to 500 km above the Earth's surface, are important even during local night time, when contributions from *Sq* and EEJ are absent.

As the ionospheric fields at polar latitudes are always present, either at quiet times or at the nightside hemisphere, it is very difficult to separate their contribution with data selection. Therefore it is critical to understand the polar ionospheric currents to improve internal field models.

2.2.2 Magnetospheric contributions

The magnetosphere is a large cavity produced by the interaction between the solar wind and the Earth's magnetic field. Essentially, the moving charged particles of the solar wind are decelerated by the magnetic pressure of the Earth's geomagnetic field and are deflected around the Earth. The complex interactions of the geomagnetic field and the solar wind give rise to a multitude of electric current systems (figure 2.7), which flow at typical distances of 2 to 20 Earth radii. Observers close to the surface, like ground-based magnetic observatories, see the combined effect of all the magnetospheric currents. The main magnetospheric current systems that contribute to the near Earth magnetic field are the *Chapman-Ferraro currents* (or *magnetopause currents*) flowing at the dayside on the magnetopause where they are responsible for the dayside compressed field lines and giving rise to the t*ail currents* on the nightside, the neutral-sheet currents responsible for the nearly parallel field lines in the nightside magnetosphere and the *ring current* in the equatorial plane (Kivelson and Russell, 1995), flowing westward and responsible for the decrease in Earth's magnetic field at low latitudes.

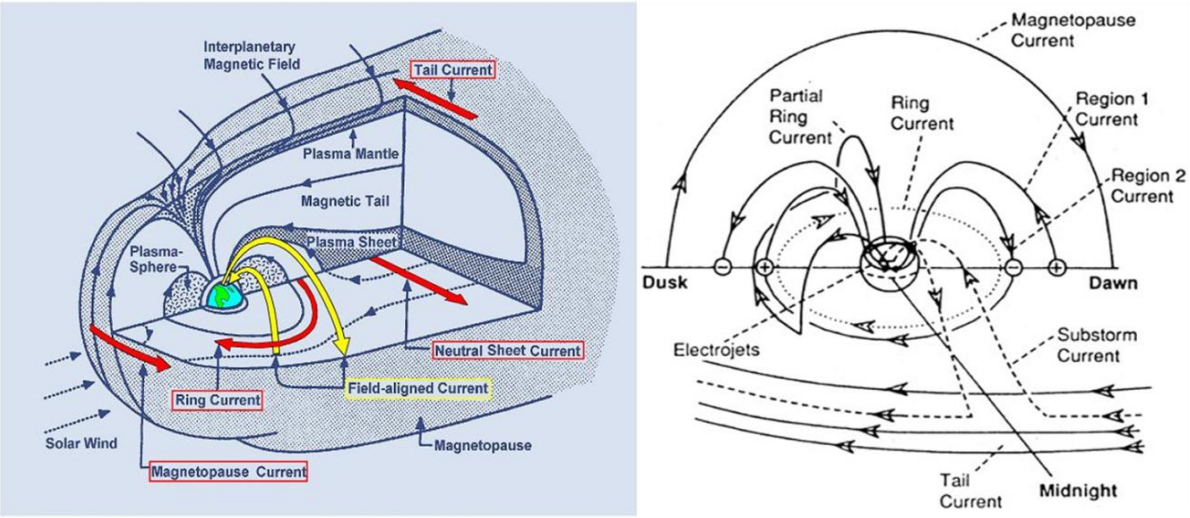

Figure 2.7. (*Left*) Sketch of the magnetosphere and magnetospheric currents. (*Right*) Highly schematic representation of the various current systems linking magnetospheric and ionospheric currents and responsible for magnetic activity (Modified after Kivelson and Russell, 1995).

The Chapman-Ferraro current cancels the Earth's field outside the magnetosphere and intensifies the field within the cavity. It flows duskward on the dayside magnetopause, around the two polar cusps (neutral points of the terrestrial magnetic field), and dawnward on the nightside magnetopause where it is called the *tail current*. The magnetic signature of the magnetopause current, at the Earth's surface, is a 24 h variation, most important on the dayside. The tail part of the current is closed inside the

magnetosphere by the so-called *neutral-sheet current*, established in the equatorial plane, which separates the Northern and Southern lobes of opposite magnetic field. The ground effect of the tail currents is a southward perturbation (Menvielle et al, 2011).

The interaction of these currents with the radiation belts closer to the Earth produces a ring current in the dipole equatorial plane which partially encircles the Earth, but achieves closure via the FAC into and out of the ionosphere (Olsen et al, 2010). The ring current flows westward around the Earth at a distance between 3 to 6 Earth radii. Its ground effect is a southward perturbation reducing the strength of the main field (on the H component), except near the magnetic poles, where it contributes mostly to the Z component. As its magnitude disturbance is proportional to the total energy of drifting particles, it's also strongly enhanced during magnetic storms and substorms when energization of these drifting particles occurs. Moreover, during substorms and the main phase of storms, the drifting ions gain energy in the nightside, this causes the ring current to be more intense near dusk, where it is called the *partial ring current*. It causes an asymmetric pattern of the ground magnetic perturbation, with more southward perturbation at the dusk than at the dawn (Menvielle et al, 2011).

The FAC are mainly composed by two concentric regions of currents encircling the Earth. They flow from the equatorial magnetosphere to the high-latitude ionosphere along magnetic field-lines. Figure 2.7 shows a schematic representation of these current systems. The two regions of FACs are as follows: Region-1 contains the most poleward currents, originated from the nightside convection in the external magnetosphere driven by reconnection in the magnetospheric tail. Region-2 contains more equatorward currents, originated from the divergence of the ring current driven by pressure gradients in the magnetospheric ring plasma. These currents flow in opposite directions on each side of the noon-midnight plane (figure 2.7) and their effects across the auroral oval cancel each other and cannot be measured on the ground. Other currents exist in the magnetosphere-ionosphere circulation, some reconnect Redion-1 and Region-2 in the auroral zone, some causing measured perturbations on the ground and other not. Additional currents occur only during magnetic storms and substorms, like the *substorm current wedge* (Menvielle et al, 2011).

2.2.3 Induction in the solid Earth and the oceans

The time-varying external fields produce secondary, induced, currents both in the Earth's interior (lithosphere) and in the oceans. This gives rise to what is called externally induced fields. The induced fields will depend on the regional conductivity of the lithosphere (Constable, 2007). In addition, the motion of electrically conducting seawater though the main field also produces secondary currents via a process referred to as *motional induced induction* (Maus, 2007; see Olsen, 1997b). As a result, the oceans contribute two times to the observed magnetic field: by secondary currents induced by primary current systems in the ionosphere and magnetosphere; and by motion-induced currents due to the movement of seawater, such as tides, relative to the main field (Olsen et al, 2010). See figure 2.6 for

an example. The amplitude of the induced contributions generally decreases with the period or the sea water velocity. Also, its effects depend on the spatial scale of the source: for example, the induced contribution due to the daily variation of the EEJ is much smaller than the contribution of the daily *Sq* variation (Olsen, 2007).

2.3 On geomagnetic indices

Geomagnetic indices are a measure of the disturbance of geomagnetic activity, which is a signature of the response of the Earth magnetosphere and ionosphere to solar forcing (Menvielle et al, 2011). The International Association of Geomagnetism and Aeronomy (IAGA)[1] officially supports (through the International Service of Geomagnetic Indices, ISGI[2]) a number of indices. Since the second part of the twentieth century they have become a fundamental parameter in the solar terrestrial studies. In the last two decades they have become a key element in Space Weather, used to detect, describe and predict events associated with disturbances in the Earth's electromagnetic environment, which can affect more or less significantly human activities. Some indices were introduced recently. For a specific index there is an intention that it will be able to inform on the dynamics and physical origin of a specific event/process in the Earth's ionized environment (table 2.2). A classification on the geomagnetic indices may be as follows (Menvielle et al, 2011):

2.3.1 Polar and auroral indices

a) PC indices

The polar cap index (PCN: northern; PCS: southern) aims at characterizing the magnetic activity in the polar caps (latitudes > 80º). This is mainly driven by the sign of Interplanetary Magnetic Field (IMF) Bz component. When that sign is negative (in a solar-magnetospheric coordinate system[3]), consisting in a southward directed IMF, encounters the northward directed magnetic field of the Earth, then the field lines interconnect, distorting the Earth's dipole field and providing entry for the solar-wind particles into the magnetosphere. The southward turning IMF (Bz becoming < 0) is then a critical requirement for the initiation of major magnetic disturbances at the Earth, like the magnetic storms or the increase of FAC. Each index (PCN or PCS) uses the magnetic variations observed at a single near pole station (PCN: Qaanaaq, formerly known as Thule, Greenland; PCS: Vostok, Antarctica). It was first proposed by Troshichev et al. (1979, 1988). The PC index can be regarded as a measure of high-

[1] *http://www.iugg.org/IAGA/iaga_pages/pubs_prods/Products_services.htm*

[2] *http://isgi.cetp.ipsl.fr/.* All indices values can be found from here.

[3] The Geocentric Solar-Magnetospheric (GSM) coordinate system has its X-axis from the Earth to the Sun; the Y-axis perpendicular to the Earth's magnetic dipole, so that the X-Z plane contains the dipole axis, and the positive Z-axis is chosen to be in the same sense as the northern magnetic pole. By definition the Y-axis is always in the magnetic equator and it is the dawn-dusk meridian (pointing towards dusk).

latitude, transpolar convection electric fields generated by coupling of the solar wind and interplanetary magnetic field with the Earth's magnetosphere. The (complex) algorithm to derive the PC index is based on a statistical analysis of relationships between variations in the interplanetary parameters and ground geomagnetic perturbations observed near the corrected geomagnetic pole (Papitashvili et al, 2001). Vennerstrøm et al. (1991) stressed that the most serious problem is that several sources can contribute to the PC index and that it is difficult to distinguish between them.

b) Auroral-Electrojet (AE) indices

The auroral-electrojet (AE) index was originally introduced by Davis and Sugiura (1966) as a measure of global electrojet activity in the auroral zone (latitudes between 60º and 80º). The AE index is derived from geomagnetic variations in the H component (see section 3.3) observed at 12 selected observatories along the auroral zone in the Northern Hemisphere[4], over an 8º latitude range and with a longitudinal distribution. A base value for each month, from the averaging of the five quietest days, is calculated for each station to normalize the data. The AU and AL indices are respectively the largest ("Upper") and smallest ("Lower") variation values of H at each station and Universal Time (UT). The difference (AU minus AL), defines the AE index, and the mean value ($(AU + AL)/2$), defines the AO index. The AU and AL indices are intended to express the strongest current intensity of the eastward and westward auroral electrojets, respectively. The AE index represents the overall activity of the electrojets, and the AO index provides a measure of the equivalent zonal current. The "AE indices" term stands for these four indices. Many studies have been made with the AE indices, concerning the contributions of specific stations to the indices (David and Sugiura, 1966), the contributions of diurnal, seasonal and annual variations to the indices (Allen and Kroehl, 1975; Mayaud, 1980, Ahn et al, 2000) and the relation with the solar cycle (Ahn et al, 2000). Although the AE indices are manly generated from the ionospheric electrojet current, magnetospheric currents, such as the ring current, could have an effect on them. An AE index for the Southern Hemisphere was recently introduced by Weygand and Zesta (2008).

2.3.2 K index

The K index was introduced by Bartels et al. (1939) to objectively monitor the global geomagnetic activity. Since then it has been routinely used at permanent magnetic observatories, as well at temporary stations. For a full description see Mayaud (1967, 1980). Nowadays, the index can be calculated by hand-scaled magnetograms or by one of the four algorithms that are acknowledged by IAGA (Menvielle et al, 1995). The index is computed at a 3-h UT interval, and is an integer in the range 0 to 9 (10 possible values). It is a (non-linear) measure of the amplitude of geomagnetic disturbances in either of the two horizontal components during that interval, after subtraction of the

[4] Some stations have been closed and replaced by new stations. See Menvielle et al. (2011) for details.

daily variation (*Sq*). Values of K index vary between: 0-2, magnetic quietness; 3-5, moderate geomagnetic activity; 6.9, intense to very intense geomagnetic activity. The limits of classes for K indices are defined for each observatory according to a specific grid.

a) K-derived geomagnetic indices

Bartels et al. (1939) also expressed the idea to derive a planetary index of geomagnetic activity from a network of fixed observatories. Various K-derived indices exist now. These indices are derived from the Ks indices (standardized K indices) that are derived for each observatory from the corresponding K index, using conversion tables that aim to eliminate local time (LT) and seasonal effects (Bartels, 1949). The Ks index can take possible values, from 0o to 9o (0o, 0+, 1-, 1o, 1+, 2-, 2o, 2+, …, 9-, 9o). They are meaningful only at subauroral latitudes.

i) Kp (ap),and Ap indices

First introduced by Bartels (1949), the global 3-h Kp index is since then been calculated from the Ks values of 13 selected observatories[5]. The Kp index is a weighting average of Ks indices of theses 13 observatories. As already happened for K and Ks, Kp is not linearly related to the amplitudes of the geomagnetic disturbance. The ap index was introduced some years after the Kp as a way to obtain an index that was linearly related to the activity. It is deduced from the corresponding Kp through a one to one correspondence table (table 2.1; see Menvielle et al, 2011 for more details) and is expressed in "ap units": 1 ap unit ~ 2 nT. The Ap index is the daily average of the 3-h ap, also expressed in ap units.

Table 2.1. Converting from Kp to ap.

Kp	ap	Kp	ap	Kp	ap
		0o	4	0+	2
1-	3	1o	4	1+	5
2-	6	2o	7	2+	9
3-	12	3o	15	3+	18
4-	22	4o	27	4+	32
5-	39	5o	48	5+	56
6-	67	6o	80	6+	94
7-	111	7o	132	7+	154
8-	179	8o	207	8+	236
9-	300	9o	400		

ii) am, an, and as indices

Introduced by Mayaud (1968), and computed backward to start in 1959, they have continuous and homogeneous data series from 1959 to the present. The Northern and Southern Hemispheres are

[5] As in footnote 3, some stations have been closed and replaced by new stations. Moreover, some stations are heavily weighted, only two stations are in the Southern Hemisphere and seven of the four are in Europe and Northern America. See Menvielle et al. (2011) for details.

divided into longitude sectors, 5 and 4, respectively. In each sector *i*, a 3-h interval K_i value is calculated from an averaging of the individual stations K values. Then this K_i value is converted to amplitude a_i standardized for 50º corrected geomagnetic latitude and weighted in each sector. The *an* average amplitude is the a_i index in the Northern Hemisphere, and the *as* is for the Southern Hemisphere. The *am* index is the mean: $am = (an + as)/2$. All of them are expressed in nT.

iii) aλ longitude sector index

Proposed by Menvielle and Paris (2001), the $a\lambda$ is calculated from the same longitude sector as those used for the am derivation. The K_i averages of each sector are converted back into amplitudes using the same conversion tables as those used for am. The indices are expressed in nT.

iv) aa index

Introduced by Mayaud (1971), it has a continuous and homogeneous data series from 1868 onwards. Its purpose is to give a simple global monitoring of the geomagnetic activity, backward to the first years of the geomagnetic observatories network. The aa index is produced from the K indices of two nearly antipodal magnetic observatories in England and Australia[6]. For each 3-h interval the K indices at the two stations are converted back to amplitude, standardized for 50º of corrected geomagnetic latitude and then the aa index is the weighted average of the two values. The index is expressed in nT.

b) Classification of days

Two classifications of days are currently used. The first, proposed by Johnston (1943), is based upon comparison of Kp indices, aiming to identify the five *quietest* and five *most disturbed* days of the month. The second, introduced by Mayaud (1973), is based upon aa indices and aims to select days that are magnetically *quiet* or *very quiet*. In the first classification, the selection criteria give only a relative indication of the character of the selected days with respect to the other days of the month (Menvielle et al, 2011).

2.3.3 Storm indices

During geomagnetic storms, at equatorial and mid-latitudes, the decrease in the H component can approximately be represented by two components: the axially symmetric component (a uniform magnetic field parallel to the geomagnetic dipole axis, directed towards the south), and the asymmetric component (a longitudinally non-uniform field). Dst and SYM indices measure the magnitude of the axially symmetric component and the ASY index measure the asymmetric component.

[6] As in footnote 3, some stations have been closed and replaced by new stations. The recent ones are Hartland and Canberra.

a) Dst index

The magnetospheric ring current is assumed as the physical source of the axially symmetric component of the storm disturbance fields. The hourly Dst index was developed to measure the magnitude of the current which produces this symmetric disturbance (Sugiura and Kamei, 1991). Four magnetic observatories[7] were chosen to be used for the calculation of the index, because of the quality of observations and also because they are located sufficiently distant from the auroral and equatorial electrojets and are fairly evenly distributed in longitude. The Dst index is derived from the average of the disturbance variation of the H component at the four observatories, after subtraction of the *Sq* variation and baseline values (expressed by a power series in time). It is then weighted for normalization to the dipole equator, to correct for the fact that observatories farther from the dip equator do see weaker disturbances. Major disturbances in the index are negative, i.e., southward. Although the major contribution to the axially symmetric component of the Dst index is the magnetospheric ring current, the index also has contributions from the neutral sheet current, the increase of solar wind pressure in the magnetosphere and induced currents in the Earth. The effects of the FAC could be smeared out if a long series is taken. It should be noted that even during quiet periods there are currents in the magnetosphere contributing to the Dst index, the reason why this index is widely used to quantitatively monitor those currents. However, it is very difficult to separate the effects of each current.

b) ASY and SYM indices

Longitudinally asymmetric (ASY) and symmetric (SYM) disturbance indices were introduced and derived for both H and D components, to describe the asymmetric and symmetric disturbance fields in mid-latitudes with high-time resolution (1-min). The ASY and SYM network consists in six stations[8], evenly distributed in longitude, and four backup stations. The SYM in H is essentially the same as the Dst index. The asymmetric disturbance field has been attributed to a partial ring current. However, it has been suggested that the disturbance may be produced by a net FAC system flowing into the ionosphere near the noon and out near midnight (Nakano and Iyemori, 2003), and that those FAC and not the asymmetric equatorial current, dominate the asymmetric disturbance fields on the ground. So, we could say that, the ASY-H and ASY-D do not necessarily indicate the asymmetry of the ring current but the effects of the FAC (Suzuki and Fukushima, 1984; Nakano and Iyemori, 2005).

[7] Hermanus, South Africa; Kakioka, Japan; Honolulu, USA and San Juan, Puerto Rico.

[8] See Menvielle et al. (2011) for details.

Table 2.2. Summary of some of the geomagnetic indices, the currents or processes that they aim to monitor and the related disturbed components and influence region.

Index	Current/Process	Spatial Disturbance
PC (N and S)	Magnetic activity driven by IMF Bz	Polar caps (> 80ºN and 80ºS) disturbances
AE	Auroral electrojet (AEJ)/overall activity	H and Y component disturbances – northern auroral zone (60º- 80º)
AU	Auroral electrojet (AEJ)/eastward	H and Y component disturbances –northern auroral zone (60º- 80º)
AL	Auroral electrojet (AEJ)/weastward	H and Y component disturbances –northern auroral zone (60º- 80º)
aa	Global geomagnetic activity	Subauroral latitudes
Dst	Ring current/Geomagnetic storms	Equatorially symmetric – magnetic equator
ASY-D and -H	FAC/ Geomagnetic storms	Longitudinally asymmetric disturbances – mid to low latitudes
SYM-D and -H	Ring current/Geomagnetic storms	Longitudinally symmetric disturbances – mid to low latitudes

3. Empirical Orthogonal Functions (EOF)

Geophysical data are characterized by non-linearity and high dimensionality. Consequently, a challenging task is to find ways to reduce the dimensionality of the system to a few modes and to link them to the dynamics/physics of the system (Hannachi et al. 2007). The Empirical Orthogonal Functions analysis (EOF, also called Principal Component Analysis, PCA) is widely used by meteorologists and oceanographers as a tool for analysis of the spatial and temporal variability of the physical fields. It's in essence an exploratory method which decomposes a data set into a basis of orthogonal functions directly determined by the data itself. In other words, it transforms a set of correlated variables into a number of uncorrelated variables, called the principal components (Natalli and Mezza, 2011).

The algebraic essentials of EOF analysis can be described as follows (Preisendorfer, 1988). Let z'(t,x) be a scalar measure of a physical process at a point x (latitude and longitude) and at a time t. Let this measure be taken at a set of locations x = 1,…,p at times t = 1,…,n. The first step is to centre the time series on their time averages

$$z(t,x) = z'(t,x) - \bar{z}(t,x) \tag{3.1}$$

With,

$$\bar{z}(t,x) = \frac{\sum_{t=1}^{n} z'(t,x)}{n} \tag{3.2}$$

All the series z(t,x) consist of a collection of readings. These collections can be thought as p×1 (i.e. column) vectors $\boldsymbol{z}(t) = [z(t,1), \dots, z(t,p)]^T$ forming a swarm of points about the origin of a p-dimensional Euclidian space (E_p). Now, it is possible to construct the symmetric scatter matrix **S** ($p \times p$) in E_p,

$$\boldsymbol{S}_{p\times p} = \sum_{t=1}^{n} \boldsymbol{z}(t)\boldsymbol{z}^T(t) = \boldsymbol{Z}^T\boldsymbol{Z}. \tag{3.3}$$

This matrix has a set of p orthogonal *eigenvectors* $\boldsymbol{e}_j = [e_j(1), \dots, e_j(p)]^T, j = 1, \dots, p$. These are the "empirical orthogonal functions (EOF's)": "empirical" because they arise from data, "orthogonal" because they are uncorrelated over space:

$$\sum_{x=1}^{p} e_j(x)e_k(x) = \begin{cases} 0, & j \neq k \\ 1, & j = k \end{cases} \qquad j,k = 1, \dots, p. \tag{3.4}$$

From these $\boldsymbol{e}_j$ we can construct the *principal components* $a_j(t)$ of the data set:

$$a_j(t) = \sum_{x=1}^{p} z(t,x)e_j(x) = \boldsymbol{z}^T\boldsymbol{e}_j \qquad t = 1, \dots n\,; j = 1, \dots, p. \tag{3.5}$$

These $a_j(t)$, thought of as time series $\{a_j(t): t = 1, \dots, n\}$, have the important property of temporal uncorrelatedness, and they carry information about the variance of the data set along the directions $\boldsymbol{e}_j$:

$$\sum_{t=1}^{n} a_j(t)a_k(t) = \begin{cases} 0, & j \neq k \\ \lambda_j, & j = k \end{cases} \qquad j,k = 1, \dots, p, \tag{3.6}$$

where λ_j is the j^{th} eigenvalue of **S**. Finally, and most importantly, the original centred data set can be exactly represented in the form

$$z(t,x) = \sum_{j=1}^{p} a_j(t)e_j(x) \qquad t = 1, \dots, n\,; x = 1, \dots, p. \tag{3.7}$$

This is the essentials of the EOF technique.

By eigenvalue decomposition of the covariance matrix of z(t,x) variations, S, this technique identifies those spatial structures of the physical field variability that have dominant contribution to the total variance (given by the sum of all eigenvalues). The spatial structure of the physical field variability is represented by the eigenvector ($\boldsymbol{e}_j(x)$), called empirical orthogonal function, and its temporal evolution is described by a series of coefficients ($\boldsymbol{a}_j(t)$), called principal components. Eigenvector and principal components together are called mode. Modes are ordered according to their decreasing eigenvalues, such that the first mode represents the largest part of the variance, the next mode the second largest part, etc.

3.1 The Singular Value Decomposition of a data set

Now we derive a *fundamental property* of the principal components of the *n*×*p* data set z. The principal components collection are pairwise uncorrelated and, as said before (equation 3.6) so,

$$\sum_{t=1}^{n} a_j(t)a_k(t) = \lambda_j \delta_{jk}. \tag{3.8}$$

On the other hand, the *total scatter* of the data set is given by (using (3.4), (3.6) and (3.7)),

$$\sum_{x=1}^{p}\sum_{t=1}^{n} z^2(t,x) = \sum_{x=1}^{p}\left[\sum_{t=1}^{n}\left[\sum_{j=1}^{p} a_j(t)e_j(x)\right]^2\right] = \sum_{x=1}^{p}\left[\sum_{j=1}^{p}\lambda_j e_j^2(x)\right] = \sum_{j=1}^{p}\lambda_j \tag{3.9}$$

Equation (3.9) shows that the total scatter of the data set is given by the sum of the eigenvalues of **S**. It also shows how the temporal variance of $z(t,x)$ at a spatial point x is weighted by the components $e_j^2(x)$, which for fixed x sum to 1 over all j values. More precisely, the (non-negative) eigenvalue λ_j of **S** is the scatter of data z along the direction $\boldsymbol{e}_j$ in E_p.

From (3.7) and (3.9) it comes, for t = 1,…,n,

$$\sum_{x=1}^{p} z^2(t,x) = \sum_{j=1}^{p} a_j^2(t) \equiv \sum_{j=1}^{p}\lambda_j \beta_j^2(t) \tag{3.10}$$

This is a special case of the second-order property of the EOF analysis. Here, for every $\lambda_j > 0$, we have introduced the *normalized amplitude* (dimensionless principal component):

$$\beta_j(t) \equiv \frac{a_j(t)}{\lambda_j^{1/2}} \qquad j = 1,\dots,p\,;\, t = 1,\dots,n. \tag{3.11}$$

The introduction of these dimensionless principal components will help us to obtain the Singular Value Decomposition (SVD) of the data. If we define $\boldsymbol{\beta}_j \equiv \left[\beta_j(1),\dots,\beta_j(n)\right]^T, j = 1,\dots,p,$ it comes easily (in scalar and matrix form)

$$z(t,x) = \sum_{j=1}^{p} \lambda_j^{1/2}\beta_j(t)e_j(x) \qquad t = 1,\dots,n\,;\, x = 1,\dots,p \tag{3.12}$$

$$Z = B\,\Lambda^{1/2}\,E^T \qquad (n \times p) \tag{3.13}$$

This last equation constitutes a form of SVD of the data z. It has a decomposition of the data which treats equally the temporal structure (via $\beta_j(t)$) and the spatial structure (via $e_j(x)$). Moreover, the variance structure of the data is clearly visible now in the presence of $\lambda_j^{1/2}$.

3.2 The uncertainty in each eigenvalue

The set of eigenvalues $\lambda_1, \dots, \lambda_p$ provides information on the distribution of variance among different, and on the separation/degeneracy of the EOF patterns. Usually, low frequency and large scale patterns tend to capture most of the variance observed in the system. The amount of data variance explained by mode *j* can be expressed in percentage as

$$\frac{100\lambda_j}{\sum_{j=1}^{p}\lambda_j}\% \tag{3.14}$$

Furthermore, sometimes the eigenvalues are not necessarily distinct and some may have multiplicity greater than one, i.e., they degenerate. The investigation of the degeneracy requires a measure of uncertainty of each eigenvalue that reflects sampling and this is quite difficult to obtain. To compute the uncertainties $\Delta\lambda_j$ and Δe_j , we will use a rule of thumb (North et al, 1982), given by:

$$\begin{aligned} \Delta\lambda_j &\approx \lambda_j\sqrt{\frac{2}{n'}} \\ \Delta e_j &\approx \frac{\Delta\lambda_j}{\lambda_k - \lambda_j}e_j \end{aligned} \tag{3.15}$$

where λ_k is the closest eigenvalue to λ_j , and n' is the number of independent observations in the sample, also known as the effective sample size, or the number of degrees of freedom. The uncertainty in the eigenvalues is useful when attempting to physically interpret a pattern or in dimension reduction, or even when looking for a break in the spectrum. For example to keep the leading three EOFs to reduce the dimensionality it is recommended that the third eigenvalue should not be too close to the fourth or higher eigenvalues (Hannachi et al, 2007).

4. Data

4.1 Data description

The magnetic observatory data was obtained from the International Real-Time Magnetic Observatory Network (INTERMAGNET)[9]. More specifically, the daily means of the magnetic components (in the DHZ or XYZ system, see section 2.1) were taken from the World Data Centre for Geomagnetism (Edinburgh) – Geomagnetic Data Master Catalogue[10]. Two data sets were created (figure 4.1 and table A.1): the first with daily means from 23 observatories and for a 39 years interval (1963-2001), and the

[9] *http://www.intermagnet.org/Welcom_e.php*

[10] *http://www.wdc.bgs.ac.uk/catalog/master.html*

second with daily means from 56 observatories and for only a 5 years interval (1985-1989). It has to be noticed that the first data set has no magnetic observatories in South America or the Pacific Ocean.

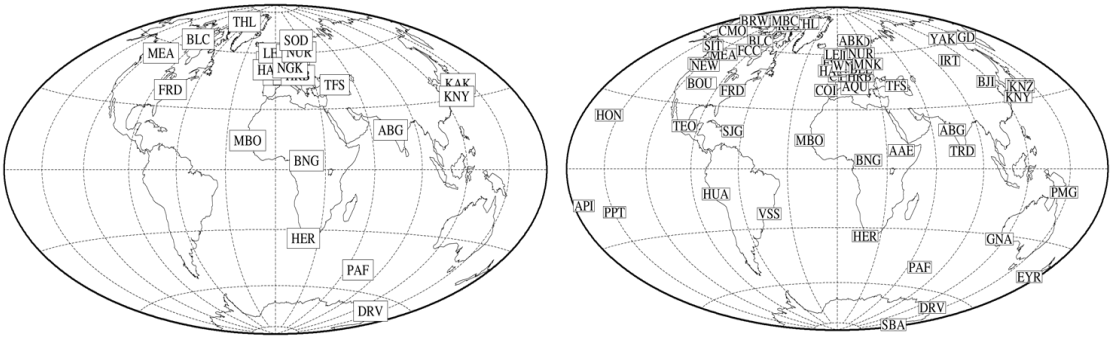

Figure 4.1. Location of the observatories used in this work. (*Left*) Observatories of the first data set (1963-2001). (*Right*) Observatories of the second data set (1985-1989).

4.2 Data pre-processing

MATLAB scripts were written to read the data from the web-downloaded files, to compute monthly and annual means from daily values and to transform data in the DHZ system to the XYZ system with the relations in equation (2.1). For some observatories the H and F components were available, for the entire period or just for some years. When this was not the case, the H and F components were computed from equations (2.4) and (2.2). Some observatory series showed occasionally very high or low spikes. Those spikes were replaced by interpolated values. The selection of the observatory data was done avoiding gaps of missing values for a great number of consecutive days. When the gap was just for one day or two a simple interpolation was done. However, for some observatories (LOV and HER) there are periods of approximately, one to three years, during which the series have values close to zero, clearly wrong, or missing values. In these cases the interpolation was done using coefficients of correlation computed with the data series from the closest observatory (figure 4.2). Assuming the coefficient of correlation *a*, between the observatory to correct (*Obs*) and the near observatory A (Obs_A), the correlation coefficient *b*, between *Obs* and the near observatory B (Obs_B) and thereafter, the correction had the form:

$$Obs(t) = a.Obs_A(t) + b.Obs_B(t) + \cdots \quad (4.1)$$

In all cases, the maximum number of near observatories used to calculate this simple interpolation was two. For example, only the near observatory NUR data series were used to interpolate the wrong values of the LOV observatory.

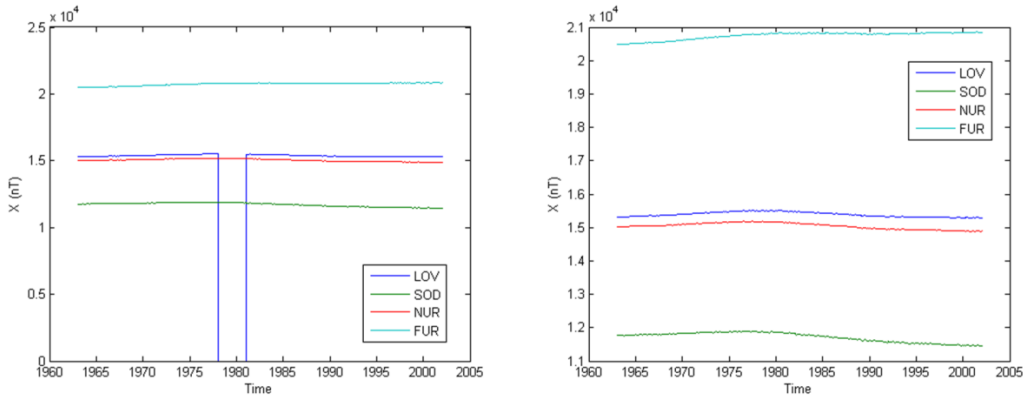

Figure 4.2. Monthly means of component X for the observatory LOV (*left*) with the initial missing values (zeros) and (*right*) after correction.

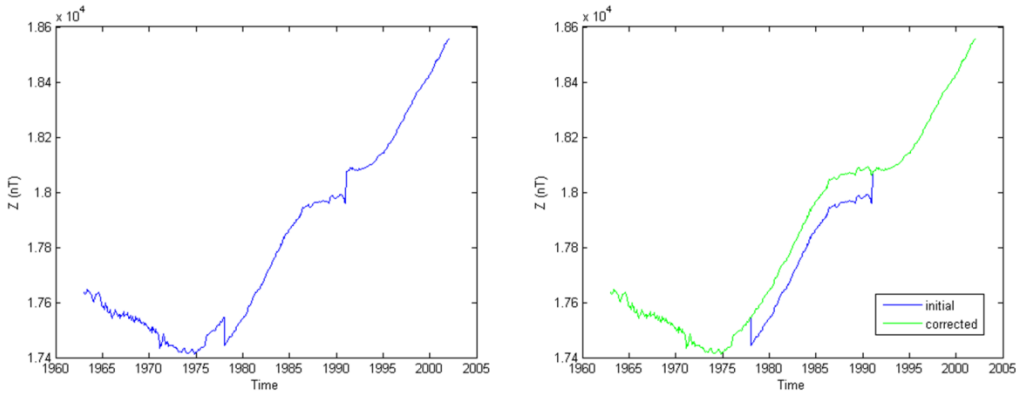

Figure 4.3. Monthly means of component Z for the observatory ABG (*left*) with the initial baseline change during a more than 10 years interval and (*right*) after correction of the baseline change.

Other aspect of the magnetic data is the baseline change/jump during some time interval. These changes are due, mainly, to substitution or some fail of the measuring instrument. One example is the ABG observatory in the X and Z components. In this case, the correction was made calculating the difference between the two periods (before and after the change) and subtracting that value in the change period (figure 4.3). Annual means were calculated from the monthly means for all components.

4.3 Removal of the internal contribution

The next step was to subtract from the magnetic components data series the contribution due to the internal (core) field. To that end, the contribution of the core field given by the CM4 model (Sabaka et al, 2004), was calculated for each observatory in use and for each year of the interval 1963-2001. Codes, input files and information for the calculations can be found on the CM website[11]. Figure 4.4 represents the contribution of the core field at the Earth's surface for the F component in 1980.

[11] *http://core2.gsfc.nasa.gov/cm/*

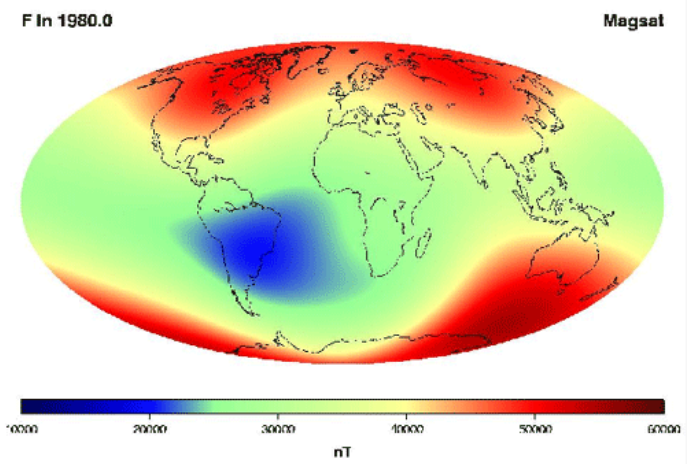

Figure 4.4. F component of the core field at the surface of the Earth, given by the CM4, in 1980. (*http://core2.gsfc.nasa.gov/CM/core.html*).

To the values obtained after subtracting the core field, we called "residuals". The main idea is that these residuals have mainly the magnetic contribution due to the external field, specifically ionospheric and magnetospheric currents. The high quality standards imposed to INTERMAGNET observatories does in principle preclude important instrumental/measuring errors. The CM4 code mentioned above gives the internal contribution for the X, Y and Z components of the field. Figure 4.5 shows an example of the residuals calculation for the HAD observatory. We can see that, as expected, the core field contribution accounts for most part of the field measured at the surface; the residuals amplitudes are in the order of tens to a few hundred nT. In the HAD observatory case, the Z component residual shows the same time increase of the field as the initial series, but for the X and Y components that does not occurs. Eventually, this could be the sign of incomplete removal of the internal signal. In the Y residuals the annual cycle is very closely sinusoidal, whereas it is much more irregular in the X and Z components. With the assumption that the residuals represent the external component of the geomagnetic field, the annual cycle is the ionospheric dynamo seasonal signature, on which the much more irregular geomagnetic storm activity superposes.

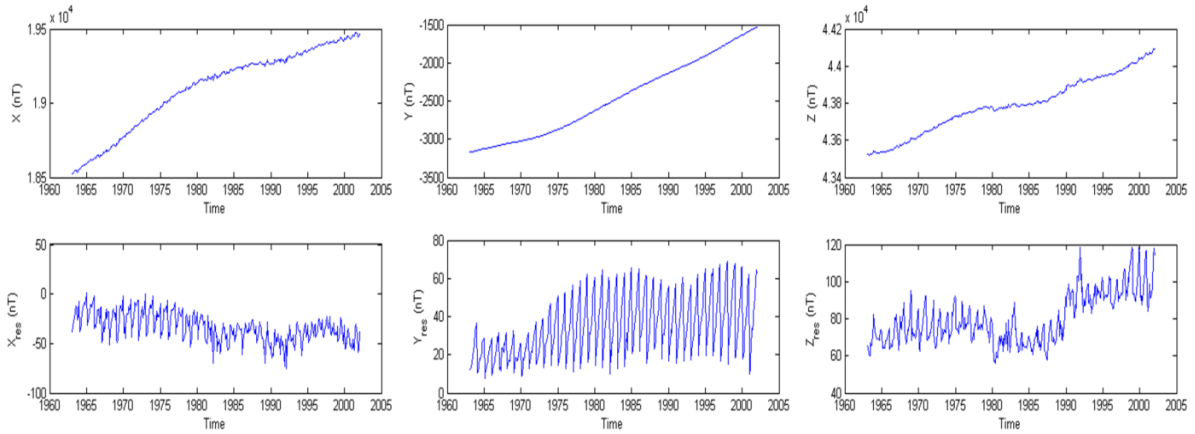

Figure 4.5. Example of the calculation of the residuals for the HAD observatory monthly means, (*top*) the initial magnetic data series, and (*bottom*) the residuals obtained after subtracting the CM4 core contribution field.

4.4 EOF analysis

The data for EOF analysis consisted in two data sets of residuals for the five magnetic components: X, Y, Z, H and F. For each component the size of the data was (following the notation in section 3):

$$\begin{aligned} n_1 = 39\,; p_1 = 23 \\ n_2 = 5\,; p_2 = 56, \end{aligned} \tag{4.2}$$

where the subscripts 1 and 2 represent the first and second data sets and the time values are for the annual means (for the monthly means the values are $n_1 = 468$ and $n_2 = 60$). Each component was organized in the matrix form (again, for the annual means):

$$Z = \begin{bmatrix} year\ 1, obs\ 1 & \cdots & year\ 1, obs\ p \\ \vdots & \ddots & \vdots \\ year\ n, obs\ 1 & \cdots & year\ n, obs\ p \end{bmatrix}_{n \times p} \tag{4.3}$$

Each row can be seen as one map of p points for an exact time, and each column as a time series of observations for a given location (Björnsson and Venegas, 1997).

After the data was subtracted from the mean, the SVD was computed for each one of the residuals matrices, for annual and monthly means and for both data sets. This involved, as a whole, the SVD of 5×2×2=20 data matrices. The result of that operation was, for each data matrix, (see equations (3.11) and (3.13)): a $p \times p$ matrix **E**, each column been an eigenvector ($e_i,\ i = 1, \dots, p$) which represents a map/spatial variability mode (that we will call EOF); a $p \times p$ matrix $\mathbf{\Lambda}$ whose square diagonal values are the eigenvalues ($\lambda_i,\ i = 1, \dots, p$) of the covariance matrix of the input residuals matrices; and finally, a $n \times p$ matrix **B** which multiplied by the $\mathbf{\Lambda}$ matrix gives the expansion coefficients ($a_t,\ t = 1, \dots, n$) (see (3.11)) or principal components (that we will call PC's). For each EOF and PC mode there is an eigenvalue that informs on the amount of variance explained by that mode.

5. Results

5.1 Amount of data variance explained

Table 5.1 represents the percentage of variance explained by the first four eigenvalues obtained by EOF analysis (given by the SVD computation) for the X, Y and Z magnetic components, the two data sets and for the monthly and annual means. The H and F components are not shown as their results do not bring something new to the discussion, i.e., they are dependent on the X, Y and Z components. The choice of showing only the first four eigenvalues is because they represent almost all variance of the data, as the summation of their values, for each component, is always more than 80% of the variance. Figures 5.1 to 5.4 show the eigenvalue spectrum obtained for all X, Y and Z matrices. All eigenvalues are represented, so the relative importance of the first eigenvalues can be understood. The eigenvalues are represented along with their standard errors as given by the first equation of (3.15),

with sample size depending on the actual size of the eigenvalues matrix, i.e., the option was to assume *n'* to be the actual sampling size of the data, even though the knowledge that the number of independent observations should be less. This means the uncertainties shown are underestimated. All the spectra have the first eigenvalues non-degenerated and separated from the rest, but overall the spectrums look in general smooth, which makes the truncation/identification of the important modes of variance difficult.

Usually, the number of eigenvalues obtained should be p (following the notation of section 4.4). However, when $n<p$, as for the case of the second data set annual means (n=5 and p=56), the eigenvalues λ_j for $j = n+1, \ldots, p$ are all zero. The MATLAB function which computes the SVD gives for these situations a 5×5 matrix **Λ**, giving only 5 eigenvalues; a 56×56 matrix **E** and a 5×5 matrix **B**. So, for the second data set annual means only five eigenvalues were obtained. For the same data set monthly means were obtained 56 eigenvalues. For the first data set 23 eigenvalues were obtained for both monthly and annual means. As can be seen in the figure 5.4 the confidence intervals for the first eigenvalues of the annual means 1985-1989 are large, consequently those eigenvalues do not have high precision.

Table 5.1. The leading four eigenvalues (expressed in percentage) of each magnetic component, for the two data sets, obtained by SVD.

Magnetic Component	Eigenvalue (%) - (explained variance)			
	1963-2001		1985-1989	
	Monthly means	Annual means	Monthly means	Annual means
X	44.14	48.13	77.13	90.69
	22.52	28.82	19.69	8.34
	12.49	7.57	1.84	0.79
	7.29	5.45	0.45	0.18
Y	67.83	46.27	92.46	98.03
	9.99	19.82	6.62	1.76
	4.81	10.32	0.27	0.18
	4.39	8.84	0.21	0.03
Z	40.99	55.39	98.21	99.62
	25.04	15.99	0.75	0.24
	9.41	10.58	0.42	0.14
	8.65	5.61	0.17	~ 0

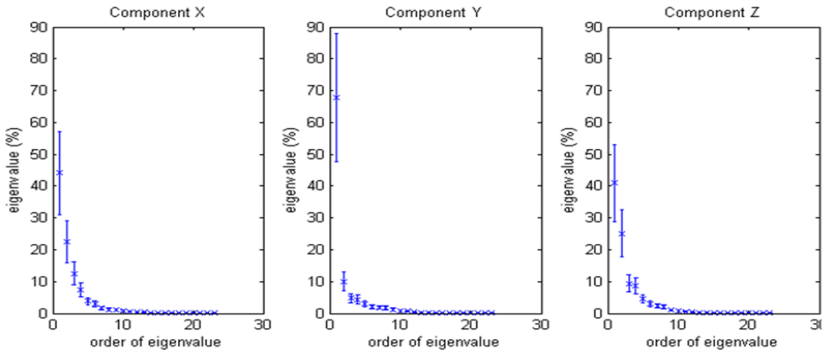

Figure 5.1. Eigenvalues spectra (expressed in percentage) for the X, Y and Z magnetic components of the monthly means first data set (1963-2001). Vertical bars show approximate 95% confidence limits given by the rule of thumb (3.15).

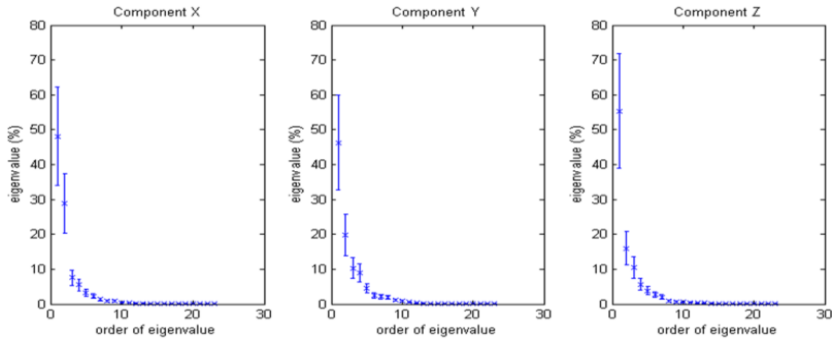

Figure 5.2. Same as in figure 5.1 but for the annual means of the first data set (1963-2001).

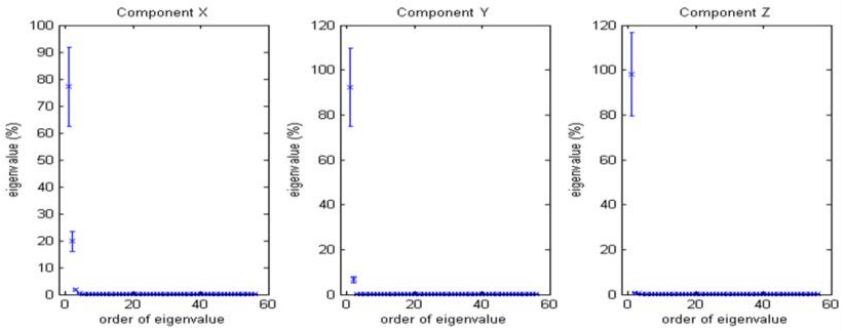

Figure 5.3. Same as in figure 5.1 but for the monthly means of the second data set (1985-1989).

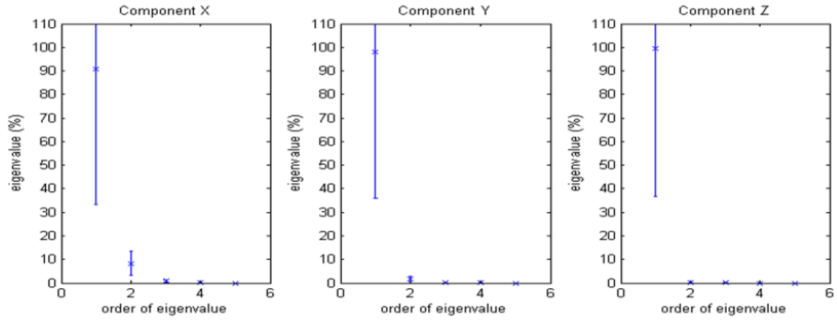

Figure 5.4. Same as in figure 5.1 but for the annual means of the second data set (1985-1989).

The main idea is to reduce the dimensionality of the system that constitutes the spatial and temporal behavior of the (external contributions for the) magnetic components. As regards the first data set (1963-2001), the first and second modes EOF explain most of the variance of the annual mean magnetic components. The monthly means of the Y residuals (figure 5.1), have a non-degenerate first eigenvalue which explains almost 68% of the variance of the Y component (see also table 5.1). So, this Y component behavior could be explained only by the first mode of variance: the time dependence by the first principal component (PC), and the spatial features by the first EOF. For the same data set, the X component monthly means (figure 5.1) and the Z component annual means (figure 5.2) eigenvalues have a difficult eigenvalue spectrum reduction. Their first eigenvalue is well separated from the second, but the rest of the eigenvalues have their sampling error distances very close to each other's, making difficult the separation. The choice is trickier but the first two modes seem enough to explain most of the variance. For the second data set (1985-1989) all components behavior could also be mainly explained by the first two modes.

5.2 Analysis of variability modes

Figures 5.5 to 5.7 display the PCs and EOFs corresponding to the most significant modes of variance (as expressed by the eigenvalues values, see table 5.1 and figures 5.1. to 5.4) for the X, Y and Z components. For the same component, the corresponding PC and EOF are shown together, firstly for the monthly means of the data set one (1963-2001), then the annual means, followed by the monthly and annual means of the second data set (1985-1989). Table 5.2 shows the amplitude intervals for each of the magnetic component residuals (X, Y and Z) field given by the first and second modes of variance, i.e. given by the relation (3.7).

As a first approach, only from the simple visualization of the results, some interesting things can be said. The EOFs of the X component have a strong geomagnetic latitudinal dependence, equatorially asymmetric, implying dependence on the polar ionospheric currents and field-aligned currents. They also show a good geographical localization of the geomagnetic poles. This occurs in the first mode (explained variance of 44% and 48%, on monthly and annual means, respectively) for the first data set (figure 5.5 (a) and (b)). The second mode (explained variance of 23% and 29%, on monthly and annual means, respectively) also shows a latitudinal dependence. Going from monthly to annual residuals, the amplitude of the first two modes decreases and the geographical localization of the geomagnetic poles deteriorate. The PC for mode 1 of the X component shows an increase of the amplitude until about 1986, with a decrease from the year 1990. The PC of the second mode shows an increase of amplitude from, approximately, 1986.

In the second data set (figures 5.5 (c) and (d)) with more observatories, among which some in Central and South America, the X component spatial pattern becomes different. Both EOF modes 1 and 2 show a strong feature in the South America region (~ -0.6 nT), which seems to control completely the

EOF1 in both monthly and annual modes. For this shorter data set, PC1 and PC2 for the annual means of the X residuals also show some change in trend around 1986.

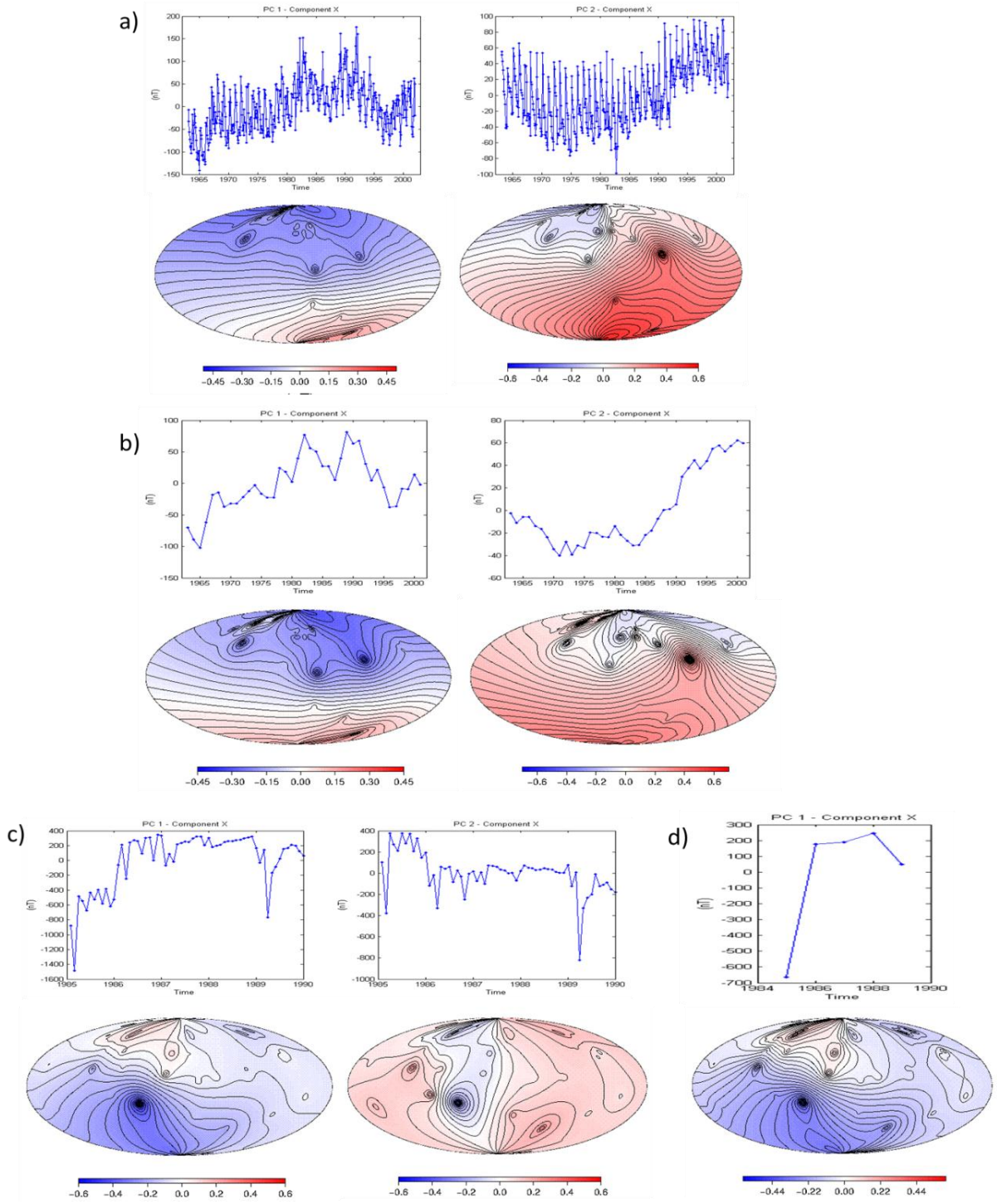

Figure 5.5. Principal components (PCs, *top*) and EOFs (*bottom*) corresponding to the most significant modes of variance for the X component (see table 5.1 and figures 5.1 to 5.4). Results for the first data set (a) monthly and (b) annual means; and for the second data set (c) monthly and (d) annual means.

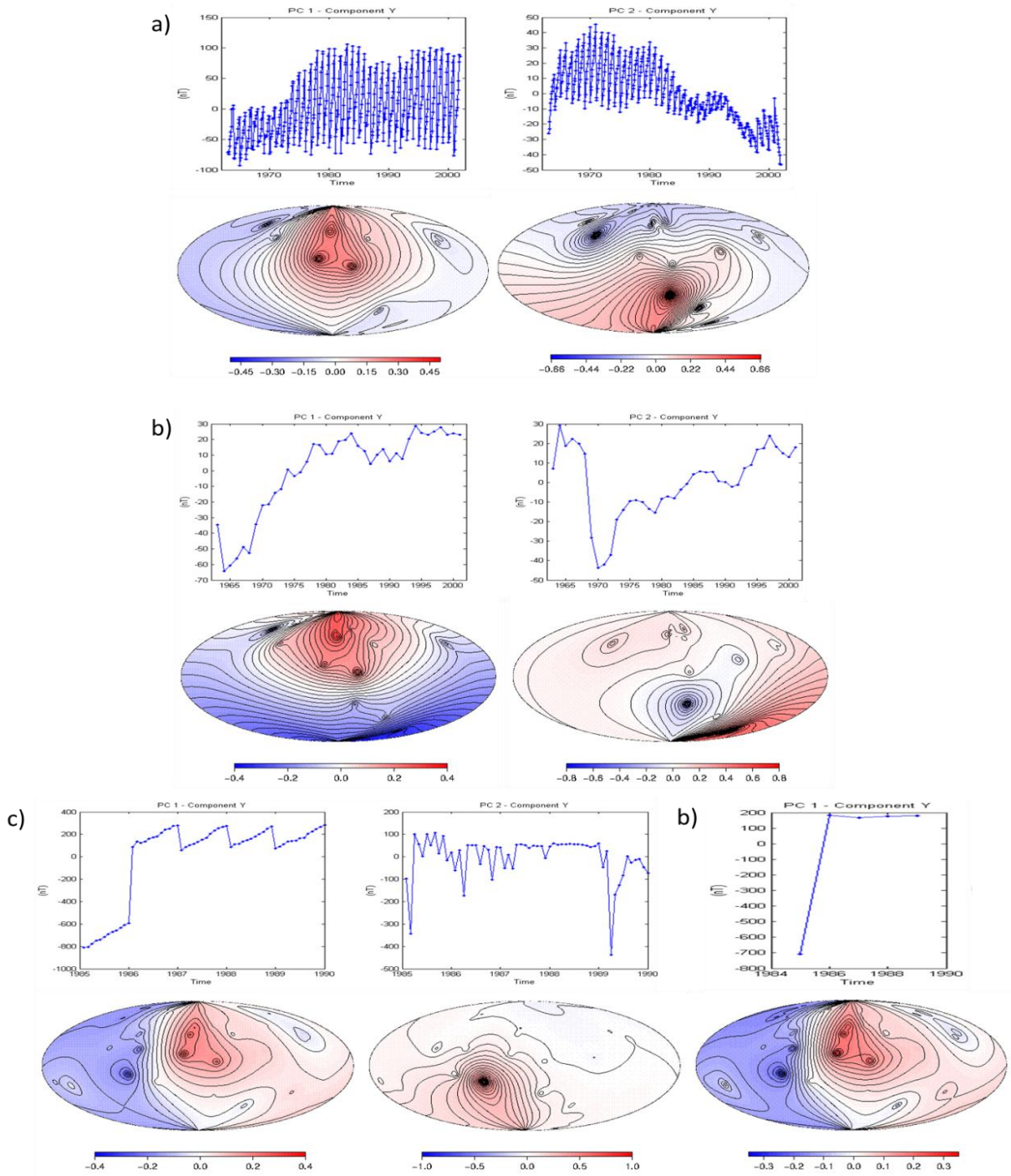

Figure 5.6. Principal components (PCs, *top*) and EOFs (*bottom*) corresponding to the most significant modes of variance for the Y component (see table 5.1 and figures 5.1 to 5.4). Results for the first data set (a) monthly and (b) annual means; and for the second data set (c) monthly and (d) annual means.

On both data sets, the EOF1 for the Y component (figure 5.6) has the same spatial pattern, a longitudinal variance, with a positive sign in the central part of the Northern Hemisphere and part of the Southern. In the monthly means of the first data set (figure 5.6 (a)) this first mode accounts for almost 68% of the variance of the Y component, but for the annual means (figure 5.6 (b)) it accounts "only" for 46%. On the other hand, in the second data set (figure 5.6 (c) and (d)) the mode 1 of the Y component corresponds to 92% of the variance in the monthly means. So, this spatial pattern appears

to be the one who mainly drive the variance of the Y magnetic component. The PC1 of the monthly means for the Y component also has a very regular annual cycle on both data sets. In the annual means the PC1 amplitude increases significantly after 1970 and stabilizes around 1986. In the mode 2 the spatial pattern is quite different, with a very strong amplitude signal in the south of Africa (first data set) and South America (second data set). This strong amplitudes control the EOF2 pattern. Besides that, the PC2 has a strong decrease around 1965 and then another strong increase from 1970.

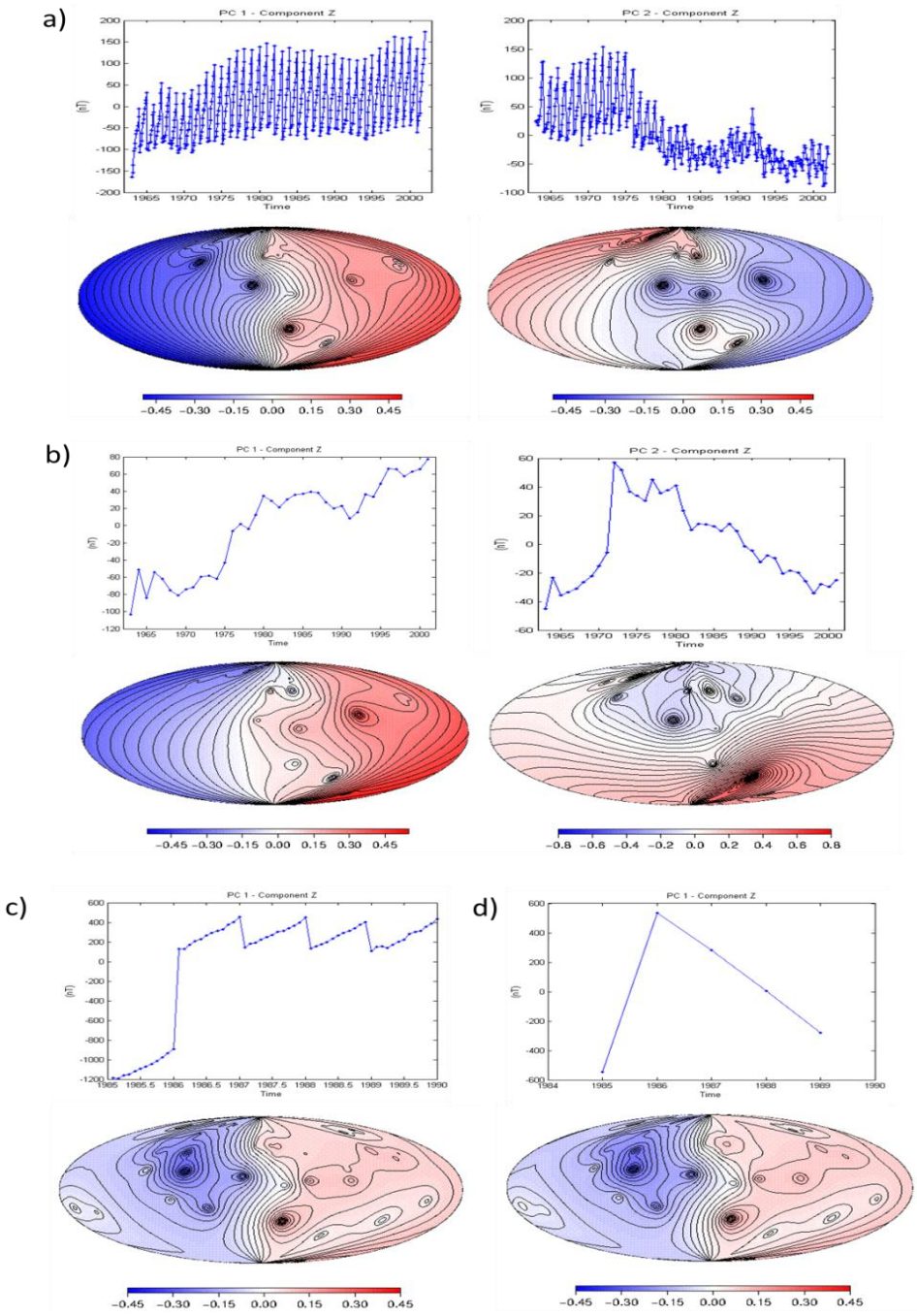

Figure 5.7. Principal components (PCs, *top*) and EOFs (*bottom*) corresponding to the most significant modes of variance for the Z component (see table 5.1 and figures 5.1 to 5.4). Results for the first data set (a) monthly and (b) annual means; and for the second data set (c) monthly and (d) annual means.

The EOFs of the Z component (figure 5.7) vary with the longitude (except EOF2 and EOF3 of the first data set annual means, figure 5.7 (b)). The (longitudinally extending) Atlantic Ocean seems determinant to this asymmetry, for which we will propose a simple explanation in the Discussion. Moreover, the monthly means PCs for the Z component show a very regular annual cycle, just like the annual cycle connected to the *Sq* field variations. This component is the one whose variance is mostly explained by the first mode alone (table 5.1). The EOF modes 1 and 2 differ almost only on the sign of the spatial pattern. Mode 1 has always a negative sign on the Western Hemisphere. However, the sign of the spatial pattern does not have a physical meaning by itself, i.e., like the relation (3.7) shows, the contribution to a magnetic component field associated with a given mode is calculated from the product of the spatial pattern of the corresponding mode and of the time series PC (Preisendorfer, 1988). So, the sign of that product is the important one (see table 5.2). In the (monthly and annual) Z component PC 1 the amplitude increases with time and in the PC2 decreases. So, the important difference between the first and second modes for the monthly Z component seems to be, besides the greater value of the mode 1 eigenvalue (41% and 25%, for the first and second eigenvalues, respectively), the spatial pattern in the geomagnetic equator (figure 5.7 (a)), which, for mode 2, changes sign at a different longitude than in the mid and high latitudes. This localized equatorial effect, which we hardly see in any other mode, suggests an influence of the equatorial electrojet (EEJ).

Table 5.2. Amplitude intervals (in nT) of the modes of variability for the X, Y and Z magnetic components residuals, for both data sets. Only the modes present in figures 5.5 to 5.7 are shown.

	1963-2001		1985-1989	
	Monthly means	Annual means	Monthly means	Annual means
X mode 1	-70 to 70	-45 to 45	-900 to 900	-434 to 434
X mode 2	-60 to 60	-36 to 36	-600 to 600	---
Y mode 1	-45 to 45	-28 to 28	-320 to 320	-245 to 245
Y mode 2	-33 to 33	-36 to 36	-450 to 450	---
Z mode 1	-75 to 75	-55 to 55	-540 to 540	-270 to 270
Z mode 2	-75 to 75	-48 to 48	---	---

In general, the PCs have bigger amplitudes in: the monthly means and in the second data set. The same is seen in the amplitudes of the modes of variability (table 5.2). Also, the first mode amplitudes are bigger than the ones from the second mode. The Y component has, in general, the smaller amplitude values, suggesting that this component variability is the less affected by the external magnetic field, as is believed by the science community. The Z component variability, on the other hand, is the most affected by the external magnetic field.

The general trends in the first data set monthly PCs seem to be the same as the annual PCs (for example, the X component monthly and annual EOF1 on the first data set, figure 5.5 (a) and (b)). For the second data set case, it's difficult to make this comparison, as the annual PCs have only five values. The EOFs are, just like the PCs, similar between the monthly and annual means. In the case of

the second data set, this similarity is even more evident. However, between the first and second data set the comparison is not so simple, the change of temporal and spatial intervals influences the results. In section 6 we will discuss this in more detail. The H and F components (not shown) EOFs are very complex and difficult to interpret, as they are formed by two or three magnetic components.

6. Discussion

We now analyse the spatial patterns of the EOFs of the X, Y and Z components (for the mode 1 and in some cases the mode 2) and try to identify spatial patterns originated by external currents. The X component patterns of EOF1 and EOF2 are mainly anti-symmetric relative to the equator. In section 6.2, some discussion on the causes of this effect is taken. The Y component shows for mode EOF1, always the same spatial pattern. As it will be seen in section 6.3, this pattern could be related with the magnetospheric ring current. The Z component presents every time the same pattern in EOF1, where longitudinal dependence is characterized by half of the globe with positive amplitude while the other half has negative one. This asymmetry could be related an effect of induction by the Atlantic Ocean. That is, as the Sq cell passes through the land and ocean, the force felt by each particle will be influenced by the direction of the induced currents in the ocean. Then, the sign of the Z component variation (as the Z component is the most affected by the induced currents in a near ocean) will be opposite in both sides of the Atlantic Ocean. Due to the lack of observatory data in the polar/high latitude zones, equatorial and Pacific regions, the spatial variance patterns in those areas are not very well defined. It is impressive how well-resolved the positing of the geomagnetic poles and equator can be, in some cases.

6.1 Dependence on temporal and spatial size of the data set

The results of the EOF analysis seem to be dependent on the spatial and temporal intervals of the studied data. This dependence on size and shape of the data by the EOF analysis is already known (Richman, 1986). The first data set gives information for a longer period of time, providing PCs with more information than the second data set.

Furthermore, the number of observatories critically influences the obtained spatial patterns, the EOFs. The EOFs of the second data set have, in general, better detail and besides that, show patterns that do not appear in EOFs of the first data set. A most noticeable example is in the Central/South America region. As the first data set has no observatories in that region, its EOFs do not show a special detail in the region. But for the second data set, which has observatories there, the detail is clear in all components.

The difference between monthly and annual means is seen in the amplitude intervals of the modes of variability (table 5.2) an also in the PCs. The annual PCs do not present an annual cycle, for obvious reasons. But the trend of the PCs, especially in the first data set is very similar between the same

components and modes, even though the amplitudes are smaller in the annual means. This should happen because the data of the annual means is smoothed by those means. Like the PCs, the EOFs are very similar between the same components. The spatial patterns have almost the same features in both monthly and annual means (for the same mode and component).

In summary, the time variation (PCs) depends on having monthly or annual means, which was expected, but the spatial variance (EOFs) does not depend much on that.

6.2 Comparing with geomagnetic indices

The principal components obtained by the EOF analysis of the residuals characterize the time variation of the data set (of each magnetic component, in this case study). From their behaviour we can get information on how or what is driving the temporal variance of each magnetic component. For example, if one PC has a strong correlation with the Dst index, that tells us that the correspondent mode of variance is strongly influenced by the magnetospheric ring current and magnetic storms. Following this idea, all PCs obtained were compared with a set of different geomagnetic indices, and also with the time series of sunspot number (SSN), which is an indicative series of the solar activity and its cycles. The series of geomagnetic indices were obtained from the ISGI website already referred in section 2.3 and the SSN monthly and annual means series were obtained from the site of the Solar Influence Data Analysis Center (SIDC)[12]. Table 6.1 illustrates the geomagnetic indices used and the time intervals for which they are available for the comparison with the PCs. Some indices, as the PCN, PCS and AE, were not available for the entire interval of 1963-2001. In appendix B the time series for these geomagnetic indices are shown. Monthly and annual means were calculated for all indices time series, and for SSN series.

Table 6.1. Summary of the geomagnetic indices used in the comparison with the PCs and the time interval of their series. The time interval of the sunspot number series (SSN) is also shown.

Index	Time interval
PCN	1975-2001
PCS	1995-2001
AE	1963-1975; 1977-2001
AU	1965-1975; 1977-2001
AL	1965-1975; 1977-2001
AO	1965-1975; 1977-2001
aa	1963-2001
Dst	1963-2001
ASY/SYM -D and -H	1981-2001
SSN	1963-2001

[12] *http://sidc.oma.be/sunspot-data/*

The comparison was made through the computation of the correlation coefficient between each PC and each geomagnetic index and SSN. Supposing we have two time series *A* and *B*, with *n* measurements written as a_i and b_i where $i = 1, \dots, n,$ then the *sample correlation coefficient* (Pearson's correlation) between the two series is written:

$$\rho_{ab} = \frac{\sum_{i=1}^{n}(a_i - \bar{a})\left(b_i - \bar{b}\right)}{\sqrt{\sum_{i=1}^{n}(a_i - \bar{a})^2 \sum_{i=1}^{n}\left(b_i - \bar{b}\right)^2}} \tag{6.1}$$

where $\bar{a}$ and $\bar{b}$ are the sample means of *A* and *B*.

The significant results can be seen in tables 6.2 and 6.3 for the first data set and in table 6.4 for the second data set. In these tables, the correlation coefficients computed with the PC1 and PC2 are presented. No correlation concerning the PCs of the second data set (1985-1989) annual means had *p-value < 0.05*. Furthermore, for testing for the hypothesis of no correlation the *p-value* or significance level was also computed. The p-value is the probability of getting a correlation as large as the observed value by random chance, when the true correlation is zero. If the *p-value* is small, say less than 0.05, then the correlation ρ_{ab} is significant. Only the correlation coefficients with the *p-value* < 0.05, were included in tables 6.2, 6.3 and 6.4.

Table 6.2. Correlation coefficients between the Principal Components (PCs) of the first data set (1963-2001) monthly means, geomagnetic indices and SSN time series. The *p-value* for each coefficient is between brackets. The correlation coefficients with absolute values greater than 0.5 are in bold.

Geomagnetic Index /SSN time series	X PC1	X PC2	Y PC1	Y PC2	Z PC1	Z PC2
Monthly means						
SSN	0.40300 (0.00255)	-0.11209 (0.00475)	0.08791 (0.00389)	0.07773 (0.00391)	0.07365 (0.00396)	0.06927 (0.00457)
aa	**0.73954** (0.00113)	-0.26480 (0.00541)	0.17179 (0.00354)	-0.09168 (0.00467)	-0.03485 (0.00422)	-0.01027 (0.00432)
Dst	**-0.78198** (0.00762)	0.23182 (0.00328)	-0.24759 (0.00533)	0.14164 (0.00367)	-0.06937 (0.00457)	0.02081 (0.00418)
AE	**0.58810** (0.00176)	-0.33658 (0.00571)	0.22059 (0.00333)	-0.043956 (0.00446)	0.01377 (0.00421)	-0.13639 (0.00486)
AU	0.22619 (0.00331)	-0.31602 (0.00562)	0.02305 (0.00417)	0.057238 (0.00403)	-0.16138 (0.00496)	-0.09762 (0.00469)
AL	-0.41686 (0.00605)	0.17357 (0.00353)	-0.11697 (0.00477)	0.11493 (0.00378)	0.06956 (0.00398)	0.01363 (0.00422)
AO	**-0.61657** (0.00691)	0.13634 (0.00369)	-0.21380 (0.00519)	0.10732 (0.00381)	-0.07169 (0.00458)	-0.14055 (0.00487)
PCN	**0.75362** (0.00105)	-0.27314 (0.00544)	0.01188 (0.00422)	0.078968 (0.00394)	-0.16471 (0.00498)	0.2324 (0.00328)
PCS	**0.61563** (0.00164)	**-0.51104** (0.00646)	0.11382 (0.00379)	-0.0277059 (0.00439)	-0.00991 (0.00432)	0.34337 (0.00281)
ASY-D	**0.64840** (0.00150)	-0.49168 (0.00637)	-0.01283 (0.00433)	0.37107 (0.00269)	-0.17639 (0.00503)	0.48879 (0.00218)
ASY-H	**0.55314** (0.00191)	-0.20822 (0.05160)	-0.02097 (0.00436)	-0.021812 (0.00437)	-0.18387 (0.00506)	0.34680 (0.00279)
SYM-D	0.15327 (0.00362)	-0.22749 (0.00525)	-0.01074 (0.00432)	0.20389 (0.00302)	-0.08895 (0.00465)	0.14685 (0.00365)
SYM-H	**-0.68570** (0.00720)	0.40048 (0.00256)	-0.07643 (0.00460)	-0.18304 (0.00506)	0.10442 (0.00383)	**-0.51744** (0.00648)

Table 6.3. Same as table 6.2, but for the first data set (1963-2001) annual means. When *p-value > 0.05*, the correlation coefficient is not shown.

Geomagnetic Index /SSN time series	X PC1	X PC2	Y PC1	Y PC2	Z PC1	Z PC2
Annual means						
SSN	**0.53734** (0.02373)	---	0.14743 (0.0437)	---	012332 (0.04496)	0.3971 (0.04925)
aa	**0.80140** (0.01018)	---	0.47075 (0.02714)	---	0.20951 (0.04054)	0.24624 (0.03865)
Dst	---	---	---	0.22502 (0.03974)	---	---
AE	**0.77023** (0.01178)	---	**0.57553** (0.02177)	---	0.29721 (0.03064)	0.41743 (0.02988)
AU	**0.73457** (0.01361)	---	0.25779 (0.03806)	---	---	0.24704 (0.03861)
AL	---	---	---	0.04397 (0.04903)	---	---
AO	**-0.61657** (0.00691)	0.07229 (0.04757)	---	---	---	---
PCN	**0.82085** (0.00919)	---	0.09012 (0.04666)	---	---	---
PCS	**0.63967** (0.00154)	0.38506 (0.03154)	---	---	0.23146 (0.03941)	---
ASY-D	**0.64840** (0.00150)	---	---	---	---	0.27990 (0.03693)
ASY-H	**0.55314** (0.00191)	0.2272 (0.03963)	---	---	---	---
SYM-D	0.47230 (0.00271)	---	---	---	---	0.13375 (0.04442)
SYM-H	**-0.68570** (0.00720)	0.05314 (0.03830)	0.27506 (0.03718)	**0.64493** (0.01821)	**0.59188** (0.02093)	---

Table 6.4. Same as table 6.2, but for the second data set (1985-1989). When *p-value > 0.05*, the correlation coefficient is not shown. No correlation was obtained related to the PCS index due to lack of data of the index during the second data set.

Geomagnetic Index /SSN time series	X PC1	X PC2	Y PC1	Y PC2	Z PC1	Z PC2
Monthly means						
SSN	0.23242 (0.02559)	-0.38984 (0.04633)	0.38813 (0.02039)	-0.20069 (0.04002)	0.13743 (0.02086)	0.34507 (0.02183)
aa	-0.20573 (0.04019)	---	0.05935 (0.03136)	---	0.02461 (0.03251)	0.61937 (0.01269)
Dst	0.12599 (0.02913)	**0.53371** (0.01554)	-0.13635 (0.03788)	0.48611 (0.01713)	-0.0999 (0.03666)	---
AE	-0.18586 (0.03953)	0.13096 (0.02897)	-0.24147 (0.04138)	0.02754 (0.03242)	-0.27015 (0.04233)	0.19942 (0.02669)
AU	-0.091115 (0.03637)	0.24010 (0.02533)	-0.19867 (0.03996)	0.16986 (0.02767)	-0.21023 (0.04034)	-0.36876 (0.04563)
AL	0.15017 (0.02833)	-0.09386 (0.03646)	0.17529 (0.02749)	-0.01371 (0.03379)	0.18624 (0.02713)	0.02955 (0.03235)
AO	0.23296 (0.02557)	0.09567 (0.03014)	0.16619 (0.02779)	0.21477 (0.02617)	0.18912 (0.02703)	---
PCN	-0.19966 (0.03999)	---	0.10379 (0.02987)	---	0.07742 (0.03075)	0.61834 (0.01272)
ASY-D	-0.07979 (0.03599)	---	0.16153 (0.02795)	-0.45684 (0.04856)	0.13312 (0.02889)	0.38073 (0.02064)
ASY-H	-0.02897 (0.03429)	---	0.22922 (0.02569)	-0.47338 (0.04911)	0.19985 (0.02667)	0.32535 (0.02249)
SYM-D	-0.01227 (0.03374)	0.02099 (0.03263)	-0.03395 (0.03447)	0.00505 (0.03316)	-0.03428 (0.03448)	-0.25915 (0.04168)
SYM-H	0.03327 (0.03222)	0.31233 (0.02292)	-0.10171 (0.03672)	0.25114 (0.02496)	-0.070142 (0.03567)	---

The PC1 for the first data set monthly means of the X component (44% of observed variance) seems to correlate with almost all geomagnetic indices. In fact, it correlates, with similar values, with SYM-H, ASY-D and ASY-H indices. So, it correlates with both longitudinally symmetric and asymmetric disturbances in the mid-latitudes, which could be related with the FAC and/or with the asymmetry in the EEJ. The strongest correlation is with the Dst index. This component variance is then strongly due to the same source of variability as that from the magnetospheric ring current, i.e. the source mechanism is shared. Note, however, that EOF1 (or EOF2) for the X residuals does not show the same equatorial symmetry as the ring current X field (see section 6.3). The PC1 for the X component is also correlated with high latitude disturbance indices, like the AE, the PCS and the PCN, especially with the last one (ρ_{ab} ~ 0.75). We can say then, that the X component is influenced by the high latitude FAC, the AEJ and polar currents, especially in the Northern Hemisphere. Maybe these currents influence, in the auroral and polar latitudes, is the reason which the X component residuals EOFs do not show equatorial symmetry, just like it would be expected if the magnetospheric ring current was the only important process influencing the X component variability. All the same correlations occur as well for the PC1 of the annual means (48%), except for the Dst and SYM-H indices. This means that, without the annual cycle, the X component is mainly driven by the high and mid latitude disturbances, with much less influence on the ring current disturbance. The PC2 (23%) of the X component (monthly means) is significantly correlated only with the PCS index, which indicates that the influence of the FAC and other currents in the Southern Hemisphere high latitudes influence a smaller amount of the X component variance. For the second data set, the only significantly correlation with an X component PC was obtained for the PC2 (48%) of the monthly means with the Dst index. So, for a small interval of time and with monthly values, the disturbance of the ring current is important to the X component variance.

For the Y component, significant correlations were obtained only in first data set annual means. The PC1 (46%) correlated with the AE index and the PC2 (20%) with the longitudinal symmetric disturbance (SYM-H). But this correlation was not very strong (~ 0.58 and ~ 0.64, respectively). The temporal variance of the Y component is then related with the AEJ and the disturbances in the auroral region and, in a less quantity, with the symmetric disturbances of the ring current.

The Z component has a significant correlation only with the longitudinal symmetric disturbance (SYM-H), by the first data set monthly means PC2 (25%) and the annual means PC1 (55%). The correlation coefficients are however not very high, ~ -0.52 and ~ 0.59, respectively.

It should be referred that the X components PCs have good correlations with the overall activity index aa, meaning that these magnetic components depend greatly on the solar activity which is an important motor of the external field short and medium variations. This correlation relation was also found by Stewart and Whaler (1992), who applied a deterministic approach, presuming a time dependence of the external and induced fields variations (varying with aa index) and then estimated the disturbances

in each geomagnetic component at a number of observatories. In their work the disturbance to the X component was consistently negative over the whole Earth's surface (which was not obtained for this study EOFs, see section 6.3) with intensification in auroral regions (also seen in this study). This auroral regions intensification could be related with the high correlations between the X component PCs and the auroral geomagnetic indices.

6.3 Comparing with a theoretical model for the ring current

Representing the ring current field as a simple potential due to a tilted external dipole, we can calculate an approximate value of the magnetic field that will be measured on the Earth's surface due to the ring current. To represent the external dipole field a harmonic potential is used, with *n*=1 and *m*=0 or 1, given by:

$$V(r,\theta,\phi) = r[q_1^0 \cos(\theta) + q_1^1 \sin(\theta)\cos(\phi) + s_1^1 \sin(\theta)\sin(\phi)], \quad (6.2)$$

where r,θ,ϕ are the spherical coordinates at the Earth's surface R_E, where R_E correspond to the Earth's mean radius.

The values of the Gauss coefficients for the external origin field were taken from Langel (1987) for a 1980 main field model where the time variation is approximate by a linear function of the solar-terrestrial activity levels (represented by a disturbance index, Dst; see section 2.3.3):

$$\begin{aligned} q_1^0 &= 18.4 - 0.63\ Dst\ (nT), \\ q_1^1 &= -1.1 - 0.06\ Dst\ (nT), \\ s_1^1 &= -3.3 + 0.17\ Dst\ (nT), \end{aligned} \quad (6.3)$$

where the formulas apply to the quiet times of low Dst index values (Campbell, 2003).

To compute the field at the Earth's surface due to this potential, then following equation (2.6) and $\vec{B} = \nabla\vec{V}$, the following relations are used:

$$X = -B_\theta = \frac{1}{R_E}\frac{\partial V}{\partial \theta}, \qquad Y = B_\phi = -\frac{1}{r sin(\theta)}\frac{\partial V}{\partial \phi}, \qquad Z = -B_r = \frac{\partial V}{\partial r}. \quad (6.4)$$

This gives:

$$\begin{aligned} X &= -q_1^0 \sin(\theta) + q_1^1 \cos(\theta)\cos(\phi) + s_1^1 \cos(\theta)\,\mathrm{sen}(\phi) \\ Y &= q_1^1 \sin(\phi) - s_1^1 \sin(\theta) \\ Z &= q_1^0 \cos(\theta) + q_1^1 \sin(\theta)\cos(\phi) + s_1^1 \sin(\theta)\sin(\phi) \end{aligned} \quad (6.5)$$

The results obtained are shown in figure 6.1. These spatial patterns of the field generated by a magnetospheric ring current can be compared with the spatial patterns of variance of the X, Y and Z components obtained by the EOF analysis.

Analysing all the EOFs of the X component (figure 5.5), we can see one thing in common with the X component from this model: the latitudinal dependence of the patterns relative to the geomagnetic equator instead of the geographic equator, with a consequent good localization of geomagnetic poles. Due to the characteristics of a field by a single dipole, which is aligned with, though of opposite polarity to, the Earth's main field, the X component has only a negative signal, with higher amplitude in the geomagnetic equator (~ -0.6 nT), increasing (to 0 nT) towards the poles. This does not happen in the X EOFs. They have opposite signal amplitude in each hemisphere, with high values in the poles and auroral regions, actually very similar with the Z component field of this model (figure 6.1). This is in agreement with the correlations between the X component PCs and the auroral and polar disturbances indices, i.e., these disturbances enhance the X component amplitude in those regions, as already referred in section 6.2.

The Y component EOFs (mode 1) are much more similar with the global pattern of the same component in figure 6.1, given by the ring current model. The positive amplitude for longitudes around the Greenwich meridian appears in the EOFs, even though this pattern does not cover all latitudes, i.e., begins in the North Pole and ends before reaching the South Pole. But the distributions in longitude are very similar.

However, this similar spatial pattern between the Y EOFs and the Y component due to a longitudinal symmetric ring current only occurs in the first mode of variance of the magnetic component, while for the X component, the agreement in the latitudinal variance pattern occurs for both first and second mode of variance. In summary, we can say that the magnetospheric symmetric ring current disturbance influences the spatial variance of both X and Y components, and maybe say that the influence on the Y component is greater.

The EOFs for the Z component are not identical or similar with the Z component field given by this simple model of the magnetospheric ring current. The presence of the geomagnetic poles is also seen in EOF2 for the Z component (figure 5.7), eventually related to the influence of the auroral electrojets.

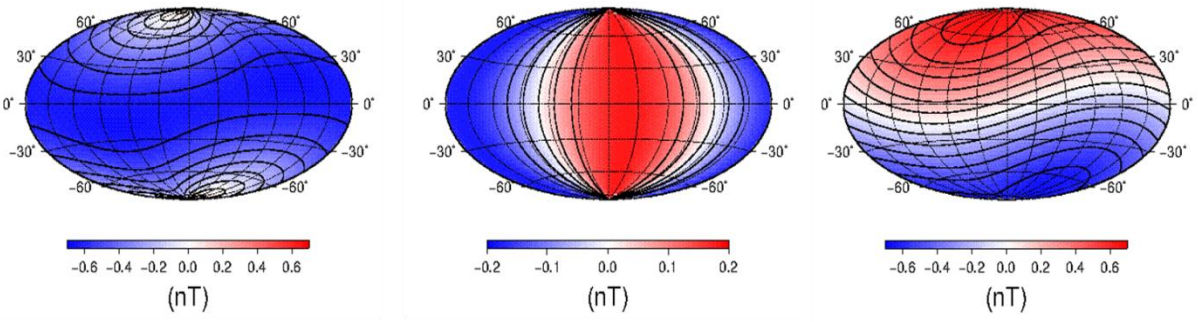

Figure 6.1. (Left) X, (center) Y and (right) Z components, measure at the Earth's surface, of the field due to a dipole centered in the Earth, as a theoretical model of the field generated by the magnetospheric ring current, given by the relations (6.5).

6.4 Comparing with the external component in the Comprehensive Model 4 (CM4)

The comprehensive model CM4, already referred in section 4.2, gives the contributions to the geomagnetic field from the magnetosphere, ionosphere, F-region FAC and others. It is interesting to compare our EOFs spatial patterns with the spatial patterns given by those contributions, especially the ones from the magnetosphere and ionosphere. Figures 6.2 and 6.3 show these contributions for different months of the year and hours of the day, respectively, at the Earth's surface.

The magnetospheric patterns (figure 6.2) are identical to the ones from the ring current model (previous section). This occurs because this contribution is parameterized in CM4 with a strong contribution from the external dipole multiplied by the time dependent Dst series (see Sabaka et al, 2002 e 2004). The positive central pattern in the Y component does not cover all latitudes, i.e. it shows some latitudinal variation, just like the mode 1 EOFs of the same component. The thing important to mention is the change of the spatial patterns during different months of the year, as the solar radiation forcing changes.

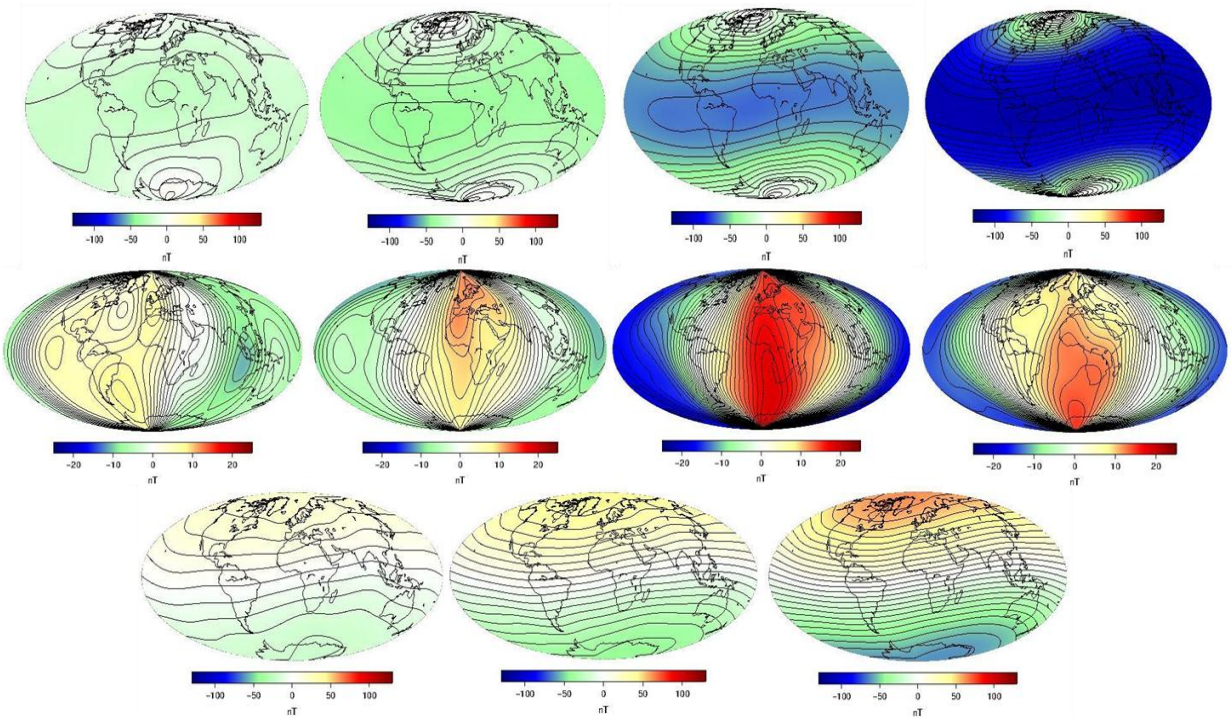

Figure 6.2. Magnetospheric contribution fields for the magnetic components X, Y and Z (*top, center and bottom row, respectively*), as given by the CM4 and for different months of the year, the first column for January and the last for June.

The ionospheric patterns (figure 6.3) are mainly controlled by the *Sq* and EEJ variations. The two images for the same component (top and bottom rows) represent two different times of the day, for the same place, recovering the day/night cycle. The X component shows high positive amplitude in the geomagnetic equator at local noon, due to the EEJ. The amplitude decreases quickly from the equator to the poles. The Y component shows lower amplitudes and a four cells pattern, characteristic of the Y

component due to the *Sq* current system (Pham Thi Thu et al, 2011). The polar regions have high (negative) amplitudes, related with the polar FAC. It's clear, in all three components, that the geomagnetic equator is not parallel with the geographic equator. The higher (negative) amplitude on the four cell pattern occurs on the geomagnetic equator over the Atlantic, exactly the place where the geomagnetic and geographical equators deviate significantly. The Z component has a pattern which depends on the latitude, with the negative amplitude in one hemisphere and positive in the other hemisphere.

In summary, the X component of computed EOFs shows some enhancement of the amplitudes in the geomagnetic equatorial zone, probably due to the EEJ, as in figure 6.3. The Y and Z component EOFs do not show patterns analogous to the ones of the ionospheric currents.

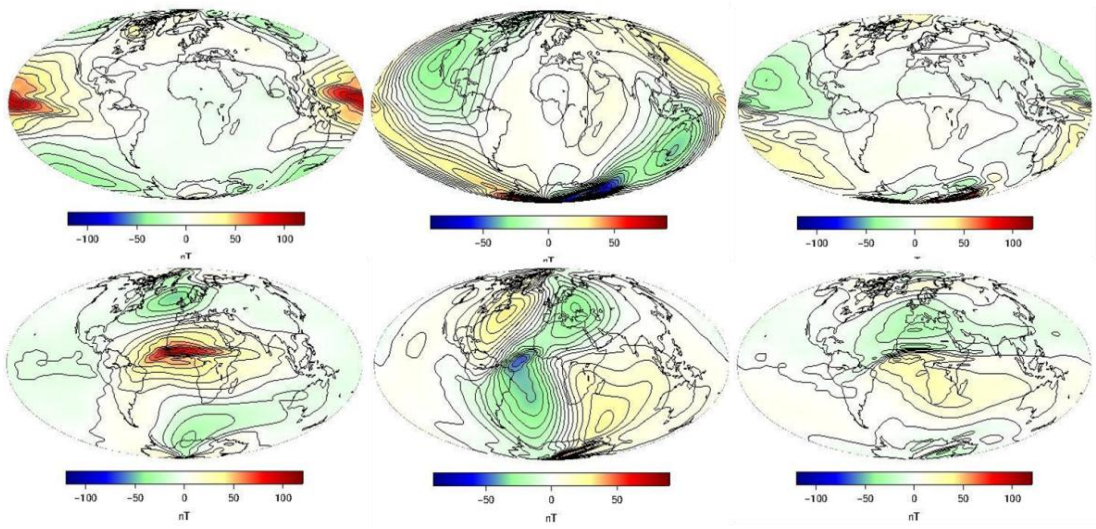

Figure 6.3. Ionospheric contribution fields for the magnetic components X, Y and Z (*left, center and right column, respectively*), for two times of the day (first row: dawn and second row: noon, at Greenwich), as given by the CM4.

6.5 Is the internal contribution still present?

The analysis of the EOFs (figures 5.5 to 5.7), especially the ones from the second data set, originated the question about the subtraction of the main field. The strong amplitude pattern in the South America/South Atlantic, present in practically all the second data EOFs seems very identical to the minimum anomaly present in the CM4 F component of the main field, in figure 4.4. This negative intensity anomaly localized in the South Atlantic region, is known as the South Atlantic Anomaly (SAA).It is known that this minimum has been slightly growing in size (Olsen et al, 2007). The whole main field influences the near-Earth magnetospheric environment, as it's its first and important source. Therefore, this SAA anomaly will also influence the magnetospheric currents. It's then difficult to assert if the negative pattern in the EOFs is due to insufficient subtraction of the main field or if it is due to induced currents in the magnetosphere due to the minimum anomaly of the main field. Other

detail is that, if as believed the SAA growing is very slow in time, it wouldn't be noticed in time intervals as 39 or 5 years. Still, is exactly in the smaller time interval that the EOFs have a pattern very similar with the SAA pattern. SAA spatial variation thus has a temporal behaviour much faster that usually thought. A way to monitor this time and spatial variation of the SAA could be the introduction of a new geomagnetic index, computed with the magnetic components time series of a few number of observatories already existing in the South Atlantic and South America region.

One test to the presence of some main field residuals is the search for jerk information in the PCs. As the Y component is the one where these phenomena are best detected, the secular variation was computed for the PCs of the Y component annual means, of the first data set (since the second only has five years). The resulting time series are shown in figure 6.4. PC1 and PC2 clearly show the 1969 jerk, with an abrupt "V" shape change in the series.

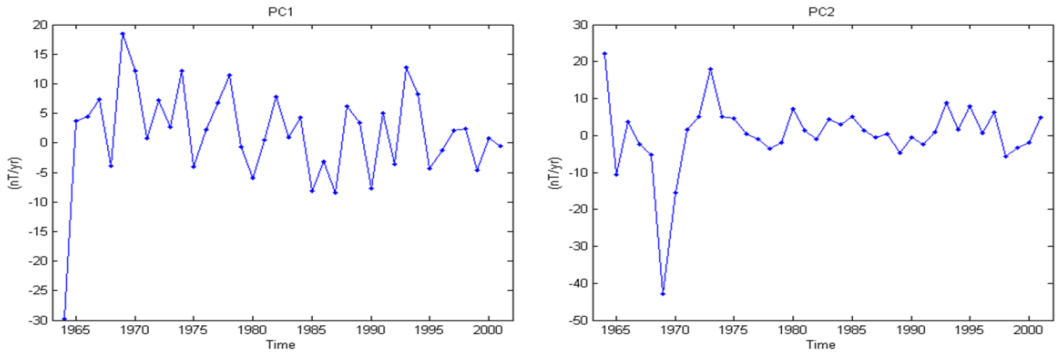

Figure 6.4. First time derivative of the principal components 1 and 2 (PC1 and PC2) of the Y component annual means, for the first data set.

Figure 6.5a) represents the global pattern of the Y component due to the 1969 jerk (Le Huy et al, 1998). Comparing with the EOF2 (correspondent to the referred PC2, figure 5.6) we see the same patterns in the South Africa region (negative amplitude) and near Australia (positive amplitude). Figure 6.5b) represents the secular acceleration (second-time derivative) for the Y component during the 1969 jerk. The global patterns in the Y component are very similar to the ones of 6.5a) and EOF2.

So, the 1969 jerk spatial pattern seems to be present in the first and second modes of the first data set. There are two possibilities: either the main field contribution was not successfully subtracted, or this main field event variation induced currents in the ionospheric and/or magnetospheric currents and these are seen in the external contribution field.

The lithospheric field contribution was not subtracted from the data series. Because we believed that its time and spatial variations were too slow to be important in a 39 or 5 years interval and in monthly and annual means. However, a more precise method should, in the future, subtract this lithospheric contribution.

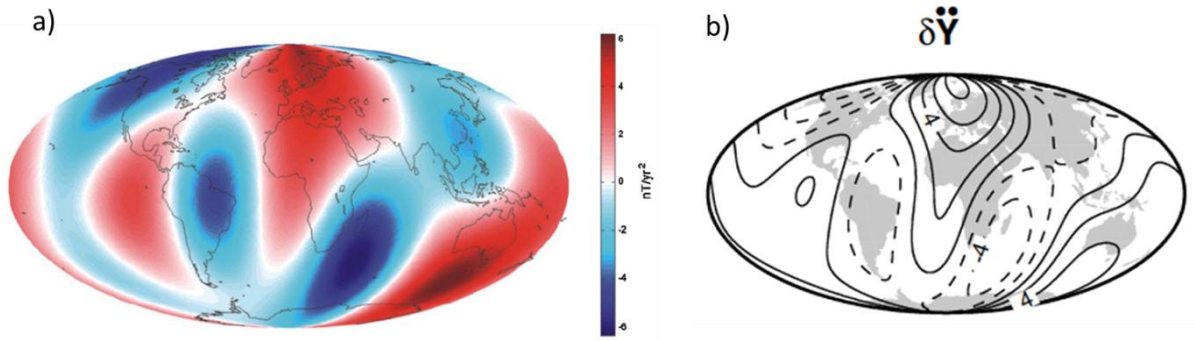

Figure 6.5. (a) Spherical harmonic model obtained from Le Huy et al. (1998) of the East (Y) component of the 1969 geomagnetic jerk at the Earth's surface (from Pinheiro and Jackson (2008)). (b) Second-time derivative (secular acceleration) of the Y components, of the 1969 jerk, given by the CM4 model. The contour interval is 2 nT/yr^2. (From Sabaka et al. (2004)).

7. Conclusions

The use of EOF analysis applied to the observatory monthly and annual means residuals allowed the identification of spatial and temporal patterns of the geomagnetic external field.

The magnetospheric ring current is an important process in the external magnetic components variability. As seen in the comparison with the spatial patterns of the X, Y and Z components due to a theoretical ring current field and the CM4 model, the ring current strongly influences the Y component. The first modes of variance of the Y component reflect that influence. These first modes account for most part of the Y variability, with 68% in the monthly and 46 % in annual means of the first data set; and also 92 % and 98% for the second data set. The X component is also related to the ring current, as the time dependence of its main mode is very well correlated with the Dst series.

The ionospheric current equatorial electrojet (EEJ) influences the spatial pattern of the X component mode 1, in the first data set EOFs.

The temporal analysis of the PCs gives insight into the importance to the auroral and polar disturbances too. Very high correlations between the PCs, especially the ones from the X component and the geomagnetic indices time series, allow us to say that this component depends greatly on the temporal behavior of the auroral electrojet (AEJ) and polar caps disturbances, as field-aligned currents (FAC). The correlation with ring current related indices, such as the longitudinal symmetric SYM and the Dst, are more important for shorter periods (the monthly means). The Y component also obtained good correlation with a ring current related index, SYM-H. The Z component has a small correlation with the SYM index, but for the EOFs patterns a correspondence with a particular current system was not obtained. Instead, a relation with induced currents on the Atlantic Ocean was suggested.

Even though the magnetospheric ring current appears as an important process influencing the magnetic components, the good correlations and spatial features in the EOFs suggest that other disturbances, especially the FAC, are important as well. More, not all magnetic components EOFS

correlated with the Dst index. So, the use the Dst index alone to parameterize the external magnetic component could not be correct. This approach is to simple, and other geomagnetic indices should be taken on.

Some EOFs showed complex patterns. Some seem to be related with the South Atlantic Anomaly (SAA) and the 1969 jerk, suggesting that there was a bad subtraction of the main field contribution, or that internal processes induced magnetic signals in the external component.

Furthermore, some EOFs appear to enclose more the effect of more than one current system, suggesting they are strongly coupled. Spatial orthogonality of the EOFs and temporal uncorrelation of the PCs impose limits on physical interpretability of EOF patterns when the physical processes are not independent. The currents of the external component seem to be related in time and space, as they induce new currents and are induced by others; and moreover with the FAC connecting two or more current systems, these currents are not completely independent from each other. Therefore, the ordinary EOF analysis may not be sufficient to correctly separate the spatial and temporal variance structures of the external sources. Other EOF methods exist and overcome some of the difficulties of the simple EOF method, like the Rotated EOFs or the Extended EOFs, see Hannachi et al. (2007) for some examples. These methods could be applied in the future to observatories means data series, in an attempt to better define the most important modes of variance of the external currents. The goal is to better understand the external currents contribution and also to identify and subtract it from the magnetic data.

8. Appendices

Appendix A

Table A.1. Characteristics of the Observatories used in this study. The information was obtained from the INTERMAGNET site and analyze of the data.

Data set	Observatory	Geodetic coordinates		Magnetic components		Missing values	Baseline change
		Latitude (ºN)	Longitude (ºE)	DHZ	XYZ		
1963-2011	ABG	18.638	72.872	*			yes
	BLC	64.333	263.967		*		
	BNG	263.967	18.567	*	*		
	CLF	48.025	2.26	*	*		
	DRV	-66.667	140.007		*		
	ESK	55.314	356.794	*	*		
	FRD	38.21	282.633	*			
	FUR	48.17	11.28		*		
	HAD	50.995	355.516	*	*		
	HER	-34.425	19.225	*	*	2000	
	HRB	47.873	18.19	*	*		
	KAK	36.232	140.186	*			
	KNY	31.424	130.88	*			
	LER	60.138	358.817	*	*		
	LOV	59.344	17.824	*	*	1978-1980	
	MBO	14.392	343.042	*	*		
	MEA	54.615	246.653	*	*		
	NGK	52.072	12.675	*	*		
	NUR	60.508	24.655		*		
	PAF	-49.353	70.262	*	*		yes
	SOD	67.367	26.633		*		
	TFS	42.092	44.705	*			
	THL	77.483	290.833	*	*		
1985-1989	ABK	68.358	18.823	*	*		
	API	-13.815	188.219	*			
	AQU	42.383	13.317	*			
	BEL	51.837	20.792		*		
	BOU	40.14	254.767	*			
	COI	40.222	351.578	*			
	CMO	64.87	212.14	*			
	FCC	58.786	265.912		*		
	GNA	-31.78	115.95	*			
	HON	21.32	202.0	*			
	IRT	52.167	104.45	*			
	KNZ	35.256	139.956	*			
	MBC	76.315	240.638		*		
	MGD	60.117	151.017	*			
	MNK	54.5	27.883	*			
	NEW	48.267	242.883	*			
	PMG	-9.408	147.152	*			
	PPT	-17.567	210.426	*			
	RES	74.69	265.105		*		
	SBA	-77.85	166.763	*	*		
	SIT	57.067	224.67	*			
	VIC	48.517	236.583	*	*		
	YAK	61.96	129.66	*			
	AAE	9.035	38.766		*		
	SJG	18.117	293.85	*	*		
	HUA	-12.05	284.67	*	*		
	WNG	53.743	9.073		*		
	EYR	-43.422	172.355	*			
	TEO	19.747	260.818	*			
	TRD	8.483	76.95	*			Yes
	BRW	71.3	203.38	*			
	BJI	40.04	116.175	*			
	VSS	-22.4	316.35	*			

Appendix B

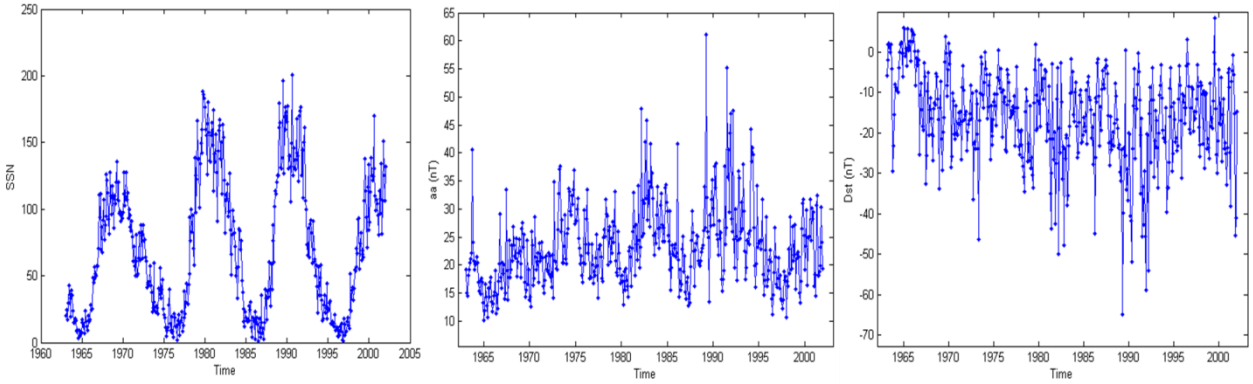

Figure B.1. (*Left*) Sunspot number and geomagnetic indices: (*center*) aa and (*right*) Dst.

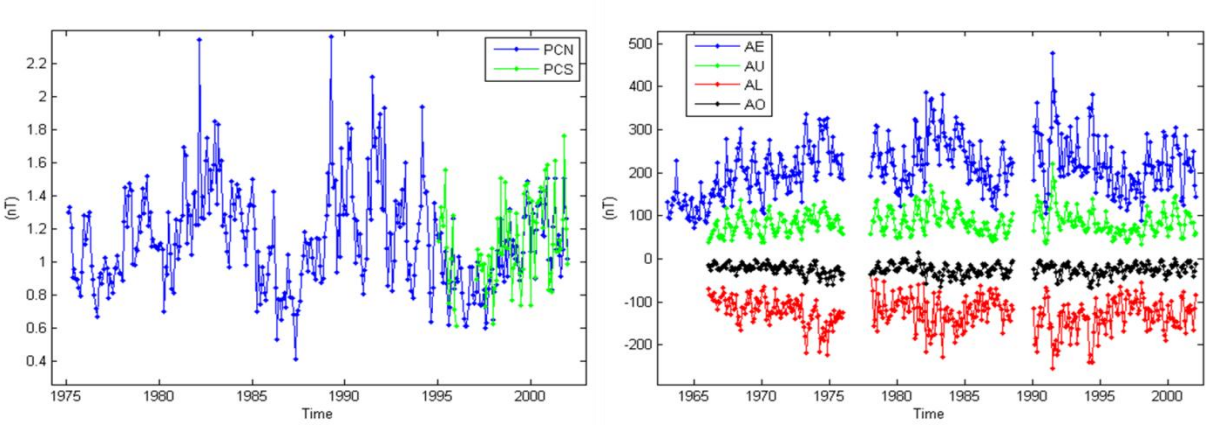

Figure B.2. Geomagnetic indices: (*left*) Polar Cap North (PCN) and South (PCS) and (*right*) AE indices. Note that the time interval is not equal in both graphics.

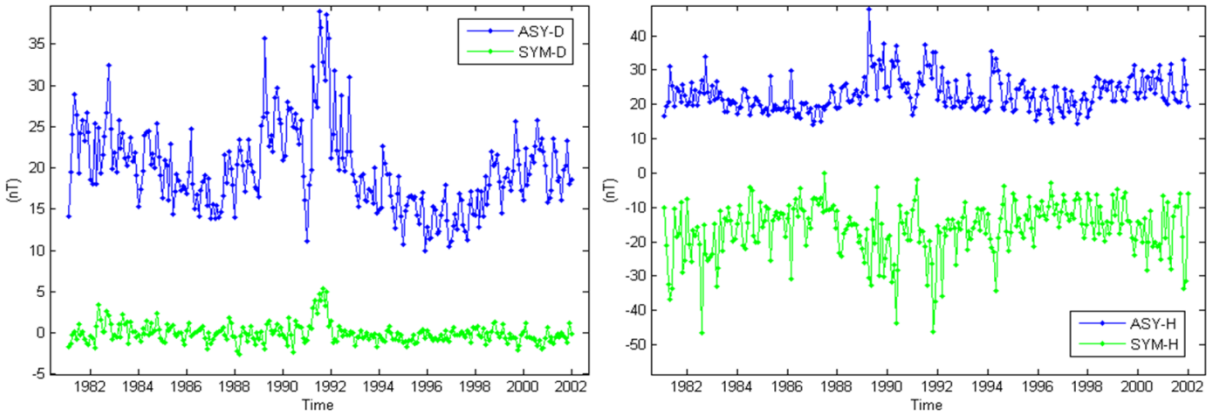

Figure B.3. (L*eft*) Longitudinal asymmetric (ASY) and symmetric (SYM) indices time series, for the D component and (*right*) for the H component.

9. References

Ahn, BH, Kroehl, HW, Kamide, Y, Kihn, EA, 2000. Seasonal and solar cycle variations of the auroral electrojet indices. *J. Atmos. Solar-Terr. Phys*, **62**, 1301-1310. DOI: 10.1016/S1364-6826(00)00073-0.

Allen, JH, Kroehl, HW, 1975. Spatial and temporal distributions of magnetic effects of auroral electrojets as derived from AE indices. *J. Geophys Res*, **80(25)**, 3667-3677. DOI: 10.1029/JA080i025p03667.

Balasis, G, Egbert, GD, 2006. Empirical orthogonal function analysis of magnetic observatory data: Further evidence for non-axisymmetric magnetospheric sources for satellite induction studies. *Geophys. Res. Lett.*, **33**, L11311. DOI: 10.1029/2006GL025721.

Barbosa, SM, Andersen, OB, 2009. Trend patterns in global sea surface temperature. *Int. J. Climatol*., **29**, 2049-2055. DOI: 10.1002/joc.1855.

Bartels, J, 1949. The standardized index, Ks, and the planetary index, Kp. IATME Bulletin 12b, 97.

Bartels, J, Hecks, NH, Johnston, HF, 1939. The three-hour-range index measuring geomagnetic activity. *J. Geophys. Res*., **44**, 411. DOI: 10.1029/TE044i004p00411.

Bjornsson, H, Venegas, SA, 1997. A manual for EOF and SVD analysis of climate data. McGill University, CCGCR Report No. 97-1, Montreal, Quebec.

Campbell, WH, 2003. Introduction to Geomagnetic Fields. Second Edition. Cambridge University Press, United Kingdom.

Constable, S, 2007. Geomagnetic induction studies. In: Treatise on Geophysics. Kono, M (Ed.). Elsevier, Amesterdam, vol. 5, 237-276.

Davis, TN, Sugiura, M, 1966. Auroral electrojet activity index AE and its universal time variations. *J. Geophys. Res*.,**71**, 785-801. DOI: 10.1029/JZ071i003p00785.

Hannachi A, Jolllife, IT, Stephenson, DB, 2007. Empirical orthogonal functions and related techniques in atmospheric science: A review. *Int. J. Climatol.*, **27**, 1119–1152. DOI: 10.1002/joc.1499.

Heelis, RA, 2004. Electrodynamics in the low and middle latitude ionosphere: a tutorial. *J. Atmos. Solar-Terr. Phys.*, **66**, 825-838.

IAGA, Working Group V-MOD. Participating members: Finlay, CC, Maus, S, Beggan, CD, Bondar, TN, Chambodut, A, Chernova, TA, Chulliat, A, Golovkov, VP, Hamilton, B, Hamoudi, M, Holme, R, Hulot, G, Kuang, W, Langlais, B, Lesur, V, Lowes, FJ, Lühr, H, Macmillan, S, Mandea, M, McLean, S, Manoj, C, Menvielle, M, Michaelis, I, Olsen, N, Rauberg, J, Rother, M, Sabaka, TJ, Tangborn, A, Tøffner-Clausen, L, Thébault, E, Thomson, AWP, Wardinski, I, Wei, Z, Zvereva, TI, 2010. International Geomagnetic Reference Field: the eleventh generation. *Geophys. J. Int*., **183**, 1216-1230. DOI: 10.1111/j.1365-246X.2010.04804.x.

Johnston, HF, 1943. Mean K-indices from twenty one magnetic observatories and five quiet and five disturbed days for 1942. *Terr. Magn. Atmos. Elec*., **47**, 219.

Kelley, MC, 2009. The Earth's Ionosphere: Plasma Physics and Electrodynamics. Second Edition. Academic Press, San Diego, CA.

Kivelson, MG, Russell, CT, 1995. Introduction to space physics. Cambridge University Press.

Langel, RA, 1987. The main field. In: Geomagnetism. Jacobs, JA (Ed.). Academic Press, New York. Vol. 1, chapter 4, 249-512.

Le Huy, M, Alexandrescu, M, Hulot, G, Le Mouël, JL, 1998. On the caracteristics of successive geomagnetic jerks. Earth Planets Space, 50, 723-732.

Lyakhov, AN, Khlybov, ES, 2006. Empirical orthogonal functions of the earth's ionosphere. *Dokl. Earth Sci*., **409**, 2, 997-999. DOI: 10.1134/S1028334X06060377.

Lorenz, E. N, 1956. Empirical orthogonal functions and statistical weather prediction. Department of Meteorology, MIT Statistical Forecast Project Rep. 1, 49 pp.

Mandea, M, Holme, R, Pais, A, Pinheiro, K, Jackson, A, Verbanac, G, 2010. Geomagnetic jerks: Rapid Core Field Variations and Core Dynamics. *Space Sci. Rev*., **155**, 147-175. DOI: 0.1007/s11214-010-9663-x.

Matsushita, S, 1967. Solar quiet and lunar daily variation fields. In: Physics of Geomagnetic Phenomena. Matsushita, S, Campbell, WH (Eds.). Academic Press, New York, chapter III-1, 301-424.

Maus, S, 2007. Electromagnetic ocean effects. In: Encyclopedia of geomagnetism and paleomagnetism, Gubbins, D, Herrero-Bervera, E (Eds.). Springer, Dordrecht, 740-742.

Mayaud, PN, 1967. Atlas des indices K. IAGA Bulletin, 21. International Union of Geodesy and Geophysics, Paris.

Mayaud, PN, 1968. Indices Kn, Ks, Km, 1964-1967. Centre National de la Recherche Scientifique, Paris.

Mayaud, PN, 1971. Une mesure planétaire d'activité magnétique base sur deux observatoires antipodaux. Ann. Geophys., 27, 67.

Mayaud, PN, 1973. A hundred year series of geomagnetic data, 1868-1967: indices aa, storm sudden commencements. *IUGG Publication Office*, Paris.

Mayaud, PN, 1980. Derivation, meaning, and use of geomagnetic indices. *Geophys. Monogr. Ser.*, vol 22, AGU, Washington, DC.

Menvielle, M, Papitashvili, NE, Häkkinen, L, Sucksdorff, C, 1995. Computer production of K indices: review and comparison of methods. *Geophys. J. Int*., **123**, 866-886. DOI: 10.1111/j.1365-246X.1995.tb06895.x.

Menvielle, M, Paris, J, 2001. The aλ longitude sector geomagnetic indices. *Contrib. Geophys. Geod*., **31**, 315-322.

Menvielle, M, Iyemori, T, Marcahudon, A, Nosé, M, 2011. Geomagnetic Indices. In: Geomagnetic Observations and Models. Mandea, M, Korte, M (Eds.). *IAGA Special Sopron Book Series 5, Springer Science and Business Media*, chapter 8, 183-228. DOI: 10.1007/978-90-481-9858-0_8.

Natali, MP, Meza, A, 2011. Annual and semiannual variations of vertical total electron content during high solar activity based on GPS observations. *Ann. Geophys*., **29**, 865-873. DOI: 10.5194/angeo-29-865-2011.

Nakano, S, Iyemori, T, 2003. Local-time distribution of net field-aligned currents derived from high-altitude satellite data. *J. Geophys. Res*., **108**, 1314. DOI: 10.1029/2002JA009519.

Nakano, S, Iyemori, T, 2005. Storm-time field-aligned currents on the nightside inferred from ground-based magnetic data at midlatitudes: Relations with the interplanetary magnetic field and substorms. *J. Geophys. Res*., 110, A07216. DOI: 10.1029/2004JA010737.

North, GR, Bell, TL, Cahalan, RF, Moeng, FJ, 1982. Sampling errors in the estimation of empirical orthogonal functions. *Mon. Weather Rev*., **110**, 699-706.

Obukhov, AM, 1947. Statistically homogeneous fields on a sphere. *Usp. Mat. Nauk*, **2**, 196–198.

Olsen, N, 1997a. Ionospheric F region currents at middle and low latitudes estimated from Magsat data. *J. Geophys. Res.*, **102**, 4563-4576.

Olsen, N, 1997b. Geomagnetic Tides and Related Phenomena. In: Tidal Phenomena, Lecture Notes in Earth Sciences. Wilhelm, H, Zuern, W, Wenzel, H (Eds.). Springer, vol. 66, 261-274.

Olsen, N, 2007. Natural sources for electromagnetic induction studies. In: Encyclopedia of geomagnetism and paleomagnetism. Gubbins, D, Herrero-Bervera, E (Eds.). Springer.

Olsen, N, Hulot, G, Sabaka, TJ, 2007. The Present Field. In: Treatise on Geophysics. Schubert, G (Ed.). Elsevier, Vol. 5 (5.02), 33-75.

Olsen, N, Hulot, G, Sabaka, TJ, 2010. Sources of the Geomagnetic Field and the Modern Data That Enable Their Investigation. In: Handbook of Geomathematics. Freeden, W, Nashed, MZ, Sonar, T (Eds.). Springer-Verlag Berlin Heidelberg, chapter 5, 106-124. DOI: 10.1007/978-3-642-01546-5_5.

Olsen, N, Stole, C, 2012. Satellite Geomagnetism. *Annu. Rev. Earth Planet. Sci*., **40**, 441-65. DOI: 10.1146/annurev-Earth-042711-105540.

Papitashvili, VO, Gromova, LI, Popov, VA, Rasmussen, O, 2001. Northern Polar Cap magnetic activity index PCN: Effective area, universal time, seasonal and solar cycle variations. Scientific Report. Danish Meteorological Institute, Terrestrial Physics Division, Copenhagen.

Pham Thi Thu, H, Amory-Mazaudier, C, Le Huy, M, 2011. Sq field characteristics at Phu Thuy, Vietnam, during solar cycle 23: comparisons with Sq field in other longitude sectors, *Ann. Geophys*., **29**, 1-17. DOI: 10.5194/angeo-29-1-2011.

Pinheiro, K, Jackson, A, 2008. Can a 1-D mantle electrical conductivity model generate magnetic jerk differential time delays? *Geophys. J. Int*., **173**, 781–792.

Preisendorfer, RW, 1988. Principal Component Analysis in Meteorology and Oceanography. Elsevier, Amsterdam.

Richman, M-b, 1986. Rotation of principal components. *J. Climatol.*, **6**, 293-335. DOI: 10.1002/joc.3370060305.

Sabaka, TJ, Olsen, N, Langel, RA, 2002. A comprehensive model of the quiet-time, near-Earth magnetic field: phase 3. *Geophys. J. Int*., **151**, 32-68.

Sabaka, TJ, Olsen, N, Purucker, ME, 2004. Extending comprehensive models of the Earth's magnetic field with Ørsted and CHAMP data. *Geophys. J. Int.*, **159**, 521-547. DOI: 10.1111/j.1365-246X.2004.02421.x.

SIDC-team, World Data Center for the Sunspot Index, Royal Observatory of Belgium, *Monthly Report on the International Sunspot Number*, online catalogue of the sunspot index: http://www.sidc.be/sunspot-data/1963-2001.

Stewart, DN, Whaler, KA, 1992. Geomagnetic disturbance fields: an analysis of observatory monthly means. *Geophys. J. Int*., **108**, 215-223. DOI: 10.1111/j.1365-246X.1992.tb00851.x.

Sugiura, M, Kamei, T, 1991. Equatorial Dst index 1957-1986. IAGA Bulletin, 40.

Suzuki, A, Fukushima, N, 1984. Anti-sunward current below the MAGSAT level during magnetic storms. *J. Geomagnetics. Geoelectrics.*, **36**, 493-506.

Troshichev, OA, Dmitrieva, NP, Kuznetsov, BM, 1979. Polar cap magnetic activity as a signature of substorm development. *Planet Space Sci*., **27**, 217-221.

Troshichev, OA, Andrezen, VG, Vennerstrøm, S, Friis-Chritensen, E, 1988. Magnetic activity in the polar cap: A new index. *Planet. Space Sci*., **36**, 1095-1102.

Tsyganenko, N. A. (1996), Effects of the solar wind conditions on the global magnetospheric configuration as deduced from data-based field models. In: Proceedings of the Third International Conference on Substorms (ICS-3), Versailles, France, 12 – 17 May 1996. Rolfe, E, Kaldeich, B, (Eds.). *Eur. Space Agency Spec. Publ., ESA-SP*, **389**, 181.

Tsyganenko, NA, Sitnov, MI, 2007. Magnetospheric configurations from a high-resolution data-based magnetic field model. *J. Geophys. Res*., **112**, A06225. DOI: 10.1029/2007JA012260.

van Sabben, D, 1966. Magnetospheric currents, associated with the N-S asymmetry of *Sq*. *J. Atmos. Terr. Phys.*, **28**, 965-981.

Vennerstrøm, S, Friis-Christensen, E, Troshichev, OA, Andrezen, VG, 1991. Comparison between the polar cap index, PC, and the auroral electrojet indices AE, AL, and AU. *J. Geophys. Res*., **96**, 101.

Verbanac G, Vrsnak, B, Temmer, M, Mandea, M, Korte, M, 2010. Four decades of geomagnetic and solar activity: 1960-2001. *J. Atmos. Solar-Terr. Phys*., **72**, 607-616. DOI: 10.1016/j.jastp.2010.02.017.

Wessel, P, Smith, WHF, 1991. Free software helps map and display data. *Eos Trans. AGU*, **72**, 441. DOI: 10.1029/90EO00319.

Weygand, JM, Zesta, E, 2008. Comparison of auroral electrojet indices in the Northern and Southern Hemispheres. *J. Geophys. Res*., 113, A08202. DOI: 10.1029/2008JA013055.